R. & M. No. 3792

R. & M. No. 3792

PROCUREMENT EXECUTIVE, MINISTRY OF DEFENCE

AERONAUTICAL RESEARCH COUNCIL

REPORTS AND MEMORANDA

Comparative Performance Measurements of Two Helicopter Blade Profiles in Hovering Flight

By M. J. RILEY AND P. BROTHERHOOD

Aerodynamics Dept., R.A.E., Bedford

LONDON: HER MAJESTY'S STATIONERY OFFICE

1977

£5 net

LIST OF CONTENTS

1. Introduction

Until relatively recently most designs of helicopter, including the *Westland Wessex* on which the tests described in this paper were made, used the NACA 0012 profile for the main rotor blades. Profiles designed specifically for helicopter rotor blades can effect a better compromise of performance characteristics in the widely varying conditions of incidence and Mach number in which they operate and one of a series of such profiles, RAE(NPL) 9615[1], developed and tested two-dimensionally has been used for the *Westland Lynx*. The changes relative to the NACA 0012 profile were conservative but were intended to give all-round improvements; that is to the shock-induced limits on the advancing blade, to the retreating-blade thrust limits and to the loading that could be sustained without shock-wave drag in hover.

The behaviour of the two profiles at conditions typically encountered during hovering flight is clearly illustrated in the wind tunnel schlieren photographs (Fig. 1). They were taken at the same incidence and not, unfortunately, at the same lift coefficient, although the difference is sufficiently small for meaningful comparisons to be made. It will be seen that a well defined shock wave has developed on the NACA 0012 profile with increased thickening of the boundary layer behind it. The flow on the upper surface has become locally supersonic and the section is operating beyond the drag rise, however no equivalent shock has developed on the RAE(NPL) 9615 section. The two-dimensional tunnel results shown an increment in C_L of 0·1 for a given level of drag.

The new profile was developed as part of a continuing programme of aerofoil research[2] (at that time being done at the National Physical Laboratory, Teddington) using theoretical methods and supporting wind tunnel tests of an essentially two-dimensional nature. However, with a lack of experimental evidence on the performance of different blade profiles on a full-scale rotor, there was at that time much discussion on the validity of using two-dimensional section data in the three-dimensional environment of the rotating blade.

Blade profile characteristics are particularly important in the tip region of a rotor blade since, in hovering flight, over 50 per cent of the total lift may be concentrated in the outer 20 per cent of the blade span. This results from the fact that the velocity increases linearly towards the tip and also because large angles of incidence are induced by the rotor wake. The tip region, however, is likely to be subjected to the strongest three-dimensional effects, including those of rotation and oscillatory flow.

It was therefore felt essential to demonstrate whether the improvements in sectional performance characteristics, shown in the two-dimensional tests, were carried over to the rotor environment. This Report describes some recent work in which the characteristics of the RAE(NPL) 9615 and NACA 0012 profiles were simultaneously measured and compared during hovering flight.

The tests included detailed measurements of blade surface and wake pressure near the blade tips over a range of local lift coefficients. The techniques of measurement were somewhat novel and had certain definite advantages in terms of accuracy and economy of pressure transducers. However, the large pneumatic lags in the pressure sensing system meant the results could only be interpreted directly during hovering flight.

The opportunity was also taken to install several pressure transducers to record instantaneous surface pressures. They were positioned to investigate methods of indicating local incidence and flow separation and also gave valuable experience of mounting to minimise spurious local aerodynamic and stress induced signals. These additional measurements were invaluable in defining the fluctuating flow in which the two profiles were compared.

It was, furthermore, realised that apart from the main aim of comparing profile performance in actual flight conditions, the tests planned were likely to provide useful information on the basic aerodynamics of the blade tip.

The tests were made on a *Westland Wessex Mk. II* helicopter between October 1971 and February 1972 at R.A.E., Bedford.

2. Blade Modifications and Recording System

The blade surface pressure and wake measurements were made in hovering flight on two specially modified blades. The problem of providing a large number of pressure measuring points without adversely affecting the structural integrity of the blade was solved by mounting the pressure tubes and miniature sensors externally on the blade within the walls of a balsa wood and glass fibre fairing or 'glove'. A glove was fitted to each of the opposing tips of one pair of the four blades for a distance of approximately 1 m (Fig. 2). This construction had the further advantage that it was possible, by extending the chord length slightly, to produce a final profile to the required aerofoil section. One of the gloves was made to the RAE(NPL) 9615 profile, and the other to the NACA 0012 used on the *Wessex* helicopter. The intention was to produce smooth 'mathematical' profiles, and so practical additions such as the leading edge anti-erosion strip and the trailing edge tab were not

represented. For a few of the flight tests, roughness bands were added to both test sections to enable further comparisons with wind tunnel results to be made. The leading edge, back to 1·78 per cent on both surfaces, was coated closely with 180 size carborundum grains attached to a strip of double-sided adhesive tape.

The surface pressure distributions were determined by measuring nineteen absolute pressures suitably distributed around the chordline (Fig. 3) at radial stations of 90·0, 91·8, 94·0 and 96·2 per cent. At two of these radial positions on each blade (91·8 and 96·2 per cent) pitot tube rakes were fitted to span the wake of the aerofoils. Their associated tubes, together with those from the surface pressure holes, were routed to the rotor hub *via* the hollow blade spar.

The aerodynamic forces and moments on the blade are affected by the change of planform, the relative position of the quarter chord and the profile characteristics of the modified portions of the blades. The final choice of chord length was governed by the requirement to provide a minimum margin of fairing in which to bury the pressure tubes at the critical points on the aerofoil. Changes in pitching moment were minimised by the choice of the quarter chordline and the lift increments due to the increased chord length were offset by adjusting the no-lift angle of the test sections. The resulting balance was such that the pair of modified blades were almost identical aerodynamically and also differed little from the standard blades.

A further major modification to the blades was the re-balancing necessary to compensate for the weight of the fairing and the pitot rakes behind the blade. Consideration had to be given to the local flutter stability of each portion of blade, to the overall blade pitching moment due to coning angle, and to the changes in the blade bending frequencies of each significant mode. These conditions had to be met with the least possible increase in blade weight and flapping inertia. The blade modifications included changes to the nose balance bars installed along the whole length of the blade, and flutter conditions were satisfied at each radius. The blade twist and control loads due to the coning moment were kept within the limits set for standard blades, and the bending frequencies were, if anything, better spaced with respect to multiples of rotor speed. The increases in blade weight and flapping inertia were 3·7 and 11·8 per cent respectively. As a test of airworthiness the blades were spun on the rotor test tower at Yeovil. The tower accepts three blades and a third blade was fitted with a glove of RAE(NPL) 9615 profile and balanced to give the same values of first flapping moment and inertia. The blades were matched as a set of three and adjustments were made to the blade balance to ensure the same tip track throughout the pitch range and that the control loads were acceptable.

The pressures from the two modified blades (96 in all) were scanned by two Scanivalves at the rotor hub during a period of five seconds. One valve was used for blade surface pressures and the other for wake pressures. The reference pressure for both valves was a pitot tube outside the region of the wake on one of the rakes nearest the blade tip. The system was designed to produce an accurate comparison of mean pressure levels for the two test profiles simultaneously in the same test conditions. It was calculated and demonstrated by bench tests that an arithmetic mean pressure of high accuracy was obtained provided a sufficient reference volume was included near the pressure transducers resulting in a pneumatic time constant of approximately five seconds for each individual pressure line.

The electrical outputs from the pressure transducers were recorded on a small paper trace recorder also mounted on the rotor hub complete with amplifiers and power supply (Fig. 4). The control link with the cockpit of the helicopter was a simple 'on–off' radio-controlled switch. One of the merits of the system was that the hub unit, being self contained, needed no slip rings and could be easily adapted to fit either the rotor test tower or the helicopter.

It was not possible to scan the surface pressures at all eight spanwise stations and the four pitot rakes during one scanning cycle. During any particular flight therefore, all four pitot rakes and only one similarly positioned spanwise row of surface pressures on each blade were scanned. The remaining surface pressures were carefully taped over and exposed in single rows as required on subsequent flights.

In addition to the mean pressure measurements, instantaneous pressures were measured on four sample miniature sensors buried in the RAE(NPL) 9615 glove to evaluate their performance on a rotor blade, and to investigate methods of measuring blade incidence and stall onset. Two 'NEP' differential pressure transducers were installed, one to measure the pressure difference between 1 per cent chord on the upper surface and 5 per cent chord in the lower surface, for the incidence correlation, and the other to measure the pressure difference at 93 per cent chord to observe the stall onset. Two 'Kulite', 'thin-line' sealed transducers were mounted at 1 and 22·5 per cent on the upper surface.

Care was taken in the mounting of these sensors to prevent any transmission of the blade stresses to the diaphragm, and to prevent any distortion of the diaphragm surround by the large centrifugal forces on the blade. It was also considered important that there should be no local irregularities in the profile shape near the pressure measuring point, and to meet all these requirements each sensor was mounted in a thin rigid box

buried in the test section fairing and profiled exactly to the local surface shape. This technique had the added advantage that the sensors were less prone to accidental damage when mounted and are re-usable.

The effects of acceleration and blade stress were assessed in flight by taping over the pressure holes; there were no outputs of any significant amplitude when the pressure was excluded. The effect of temperature on sensitivity and zero drift was measured in laboratory checks; no corrections were needed for the range of temperature variation experienced in flight.

3. Test Technique

The purpose of these tests was to compare the performance of the two blade profiles in the actual rotor environment. The fact that the special blades were locally modified in weight, section and planform was bound to modify slightly the local blade loadings normally encountered on a *Wessex* helicopter in a given flight state. The important effects of rotation, unsteadiness and wake shape (*i.e.* vortex interaction) were of course still produced at the test sections at the correct Mach number and Reynolds number. It is important for these tests to consider the helicopter as a test vehicle which produced the essential requirements of the rotor environment at the test sections; differences between the test and normal blades and in the overall performance of the *Wessex* helicopter itself were of secondary importance.

The alignment of the test sections on the blades, the tracking of the rotor and the flying technique needed to achieve the required conditions will now be described.

The experiment was intended to make a simultaneous comparison of the drag of the two profiles at the same lift coefficient. Since the cambered section has a different lift curve from the NACA 0012 (as shown by tunnel tests), the symmetrical profile was built on to the blade with 1/4 degree nose down incidence relative to the blade chordline, so that for the loadings estimated for the hover case, equal lift coefficients would be achieved. In the event, an exact match was not achieved for most of the test conditions due to a minor inaccuracy in the NACA 0012 test shape, and also to the extreme sensitivity of the local loadings to minor changes in the tracking of the blades. These experimental difficulties do not detract from the comparisons made using the lift-drag polars but a range of flight loadings was necessary to effect detailed comparisons at the same lift coefficient.

Tests on the rotor tower showed that despite the difference in profile shape, the test blades could be trimmed to remain in track with each other within the normal limits for production blades, throughout the collective pitch range. As the test blades were heavier a choice had to be made of the pitch setting at which they were in track with the standard blades. They were rigged on the helicopter to come into line with the standard blades during hovering flight. In this way the majority of test conditions flown had the lowest vibration level and the normal degree of blade-vortex interaction was encountered.

On the *Wessex Mk. II* helicopter, transmission torque limitations prevented the necessary high thrust coefficients being achieved by tethered hovering at ground level so measurements were made principally during hovering at high altitude. Some measurements were made during ground runs and when hovering near the ground, and a small number in forward flight and during manoeuvres.

The main factor limiting the aircraft performance during hovering at altitude is the tail-rotor thrust limit. For some of the required test conditions, the main rotor can be considered to be operating beyond its normal design point and large increases of torque and hence tail-rotor thrust are required to trim even small increases in main rotor thrust. The tail rotor therefore set the limit to the loading which could be imposed on the test-blade profiles.

Initial attempts to hover at high altitudes were abandoned because, with the two modified blades fitted, the helicopter was subjected to an excessive level of vibration during the normal period of 'translational buffet' encountered when approaching the hover. A technique of climbing to a hover, that is allowing the translational velocity to fall to zero before the vertical velocity, gave a much smoother transition by keeping the rotor clear of wake interaction effects throughout the manoeuvre. An added advantage was that trim changes were gradual and large control position adjustments near the limiting flight conditions were avoided.

The fundamental problem in making precise high altitude hover tests is to measure and obviate the translational velocity relative to the air mass. The translational velocity was monitored by trailing a ball on a light string below the helicopter. The direction of the bow in the string is a sensitive indicator of the magnitude and direction of translational speed. An observer viewed the string through a hatch in the floor of the helicopter and relayed its position to the pilot. This technique enabled consistent hover conditions to be maintained.

To find how sensitive the blade loading conditions were to small deviations from the exact hover state a series of 'near hovers' involving various rates of climb and descent, and small forward speeds were flown. The response of the measuring system to rapid control inputs was also recorded.

4. Reduction of Results

The rotor blade tip operates in an environment which subjects it to centrifugal accelerations, the three-dimensional effects associated with large loading gradients, and except in the exact hover condition, unsteady incident flow velocities. The analysis is further complicated by the difficulty of finding the precise value of the local stream velocity relative to the blade and the local static pressure level, remembering that these quantities must be measured from a rotating system in flight.

Consider each of these points in turn. The effects of rotation are mainly confined to the boundary layer and, before the onset of separated flow, are considered of secondary importance[3]. In spite of the large gradients in radial load it was found from flow visualisation patterns on the blade that crossflow angles were small in the region of the test sections. The periodically fluctuating flow conditions encountered in near-hovering flight, although larger than anticipated, are not thought to invalidate the analysis of the section performance in terms of the mean pressures measured.

In the measurement of profile drag, the wake momentum flux analysis requires the measurement of total head and static pressure in the region of the wake of the blade. The simple 'actuator disc' model of a rotor flow postulates discontinuities of static pressure and total head in the plane of the rotor disc, and measurements of the time-averaged values of these quantities from an external (non-rotating) frame of reference would indeed reveal changes in the region of the rotor disc. However, from a frame of reference rotating with the blade, the flow is not time-dependent, and total head is uniform outside the wake region. From this frame of reference the derivation of the profile drag from the measured distributions of total head and static pressure in the wake can follow the lines of the usual wake momentum flux analysis, the only assumption being that the flow can be considered to be locally two-dimensional.

The value of the resultant velocity of the air relative to the blade is of course of major importance and must be accurately determined. Simple momentum considerations show that the swirl velocity for the rotor considered amounts to 1/2 per cent of the blade's velocity, so that, although local flow directions are significantly altered by the resultant induced flow, the magnitude of the resultant velocity is almost exactly equal to Ωr. Similarly, to the same degree of accuracy, the local static pressure can be considered to be equal to the ambient value of static pressure, and the total head to be constant outside the wake at each radius.

Due to centrifugal forces a large pressure gradient was generated along the tubes connecting the surface pressure holes to the transducers in the rotor hub. Corrections for this gradient were applied according to the method given in Appendix A, where the derivation of p/H_0 from the measured quantities is given. All the blade pressures and the wake pitot pressures were measured relative to a reference pitot tube located below the blade outside the blade's wake. Ambient static pressure was obtained from the standard aircraft pitot-static system, and local blade relative velocities were taken to be the product of rotor speed and local radius.

The wake analysis requires a further description of the local flow in addition to the framework outlined above. It is not clear in the case of a finite wing or rotor blade that a rigorous distinction can be made, from wake measurements, between the profile and induced drag components[4], but for the purpose of the present measurements the usual two-dimensional analysis is considered adequate. More important perhaps, it is necessary to assume that the viscous wake of previous blades is not included in the decrement of total head measured behind the test section. This condition will be satisfied if, as is generally assumed, the boundary layer wake of any previous blade (closely associated with its own trailing vortex sheet) is in the form of a tightly rolled up trailing vortex by the time it reaches the tip region of the succeeding blade.

Model tests on helicopter rotors[5] combined with measurements of vortex diameter and the evidence from the shape of the pressure time histories recorded in the present experiments indicate that this vortex lies clear of the following blade (below it) sufficiently far to keep the test blade just clear of the viscous wake of the previous blade.

The pitot pressure readings themselves provided further evidence that the measured wakes were not superimposed on the wakes of previous blades. Some of the pitot tubes on each rake were located outside the wake on each row, and these readings, together with the corresponding readings on the adjacent rake, and the rakes on the opposite blade, gave an indication of the gradients of total head near the test blades. The wakes of previous blades, distorted by the vortex roll-up process, must give rise to gradients of total head in their vicinity, but the measurements show no consistent evidence of these near the test blades. No significant gradients of total head, other than expected radial variations, were measured outside the wakes.

An attempt to measure the static pressure at the wake edge by a pitot-static probe on the rake was found to be subject to large stem interference errors because the probe, being subject to large accelerations on the blade, had to be very short. The rake was located 0·1 chord behind the profile, and from a knowledge of the trailing edge pressure on the blade, and existing data on the pressure distribution in the wake of a similar aerofoil in wind tunnel tests[6], it was found possible to make an accurate estimation of the necessary correction to the drag analysis. The profile drag was then calculated by the method of Lock, Hilton and Goldstein[7], which also takes into account the effects of compressibility.

Finally the mean forces and moments were derived from the measured pressures by integration. The scarcity of measured points defining the wake pitot pressure distribution prevented a realistic fit by automatic curve fitting, and a best curve was fitted by hand and integrated using a Stanley Integraph. There were, however, sufficient surface pressure points measured to use automatic cubic circle and cubic spline curve fitting techniques. The choice of curve fitting routine for each type of plot was determined by an appraisal of the realism of the result. The data reduction programme produced the curves shown in Figs. 6, 7 and 8 on an automatic graph plotter, and evaluated the integrals for lift, chordwise force and pitching moment. The lift and pitching moment were most accurately derived from the plot of $C_p\sqrt{x/c}$ against $\sqrt{x/c}$ as the curve fitting technique could more easily accommodate the leading edge suction peak shape in these parameters. The chordwise force plot, p/H_0 *v.* z/c, was improved in accuracy by estimating the stagnation point location from tunnel tests. This could be done with some certainty, and moreover the integral was found to be relatively insensitive to the number of iterations performed to achieve the final location of the stagnation point.

5. Profile Drag

5.1. Sample Wake Pitot Pressure and Blade Surface Pressure Distributions

The magnitude and distribution of pitot pressure are principal parameters in the measurement of profile drag but a knowledge of the local lift coefficient is necessary as a basis for comparison. This was obtained from integration of the corresponding surface pressure distribution which of course is also necessary for interpretation of the various features which influence profile drag. A considerable amount of data was amassed from the tests in the form of average wake and surface pressure distributions and also various instantaneous pressure measurements. A selection of time average results is presented in this section with only brief description and comment in order to give an overall picture of their range and quality. They will be discussed in more detail in later sections and used to illustrate the numerical differences in performance obtained from the complete range of test results.

A sample sequence of wake pitot pressures for the two profiles is given in Fig. 5. They cover a range of thrust coefficients and refer to measurements at a radial position 0·918 R and local Mach number 0·57. Fig. 5a shows pressures taken on the ground with the collective pitch at its lowest value; it will be seen that the pressure distributions are virtually identical for both NACA 0012 and RAE(NPL) 9615 profiles. Fig. 5b shows the pressure distributions when hovering just out of ground effect. The areas enclosed by each curve and the 'x' axis are virtually identical but both areas are slightly larger than those of Fig. 5a indicating an overall increase in profile drag at the increased thrust and local lift coefficients.

Fig. 5c shows the wake pitot pressure distributions at an ISA pressure altitude of 4000 ft. At the reduced air density, the rotor thrust coefficient and local lift coefficient have increased sufficiently to cause a general thickening of the wake and a general increase in profile drag. This is consistent with the development of the area of supercritical flow on the upper surface of both profiles and attendant increase of shock wave drag. The thickening of the wakes is more pronounced as the local lift coefficients are further increased at an altitude of 6000 ft (Fig. 5d). It will be seen that the points from the NACA symmetrical profile are well above those of the cambered RAE profile where the wake is shed from the upper surfaces (the right hand side of the pressure distributions) and that the area enclosed by the points for the NACA 0012 profile is greater than that for the RAE(NPL) 9615 profile indicating a higher drag for the former. It should be noted however that the lift coefficient of the NACA profile is consistently slightly larger than that of the RAE profile but as will be discussed later only part of the drag increase indicated is attributable to this cause.

At 8000 ft (Fig. 5e), both profiles are fairly well into drag rise conditions and the spread of the wakes and profile drag has increased further. The difference in drag between the two profiles has also increased.

A sample selection of measured surface pressure distributions is given in Figs. 6, 7 and 8, in the form of machine-plotted measured points and fitted polynomial curves. The top and centre graphs illustrate the process described in Section 4 to obtain form drag and lift coefficient respectively; the lower graphs are the more usual plots of surface pressure against chord used in discussing and interpreting flow phenomena. The 'a'

portion of each figure refers to the NACA profile and the 'b' portion to results obtained simultaneously on the RAE profile. It will be seen that the curves are well behaved with little scatter and comparable in this respect with wind tunnel results for steady two-dimensional aerofoils.

Fig. 6 gives results obtained on the ground with minimum collective pitch and low lift coefficient and are useful in establishing minimum values of profile drag coefficient.

Fig. 7 gives results obtained just clear of ground effect below drag divergence. In part (b) the pressure distribution for the corresponding NACA profile (at a slightly higher C_L value) has been superimposed.

Sample results with blades having roughened leading edges are given in Fig. 8. They were obtained at an altitude of 8000 ft with the blade tips operating well into drag rise conditions. The corresponding NACA profile results have been superimposed in section (b) and it should be noted these results are part of a small number taken with adjusted tracking in which the pitch of the NACA blade was reduced slightly. In this case the resulting lift coefficient of the NACA profile is less than that of the RAE profile.

Results (with smooth blades) of both surface and corresponding wake pressures representative of conditions below drag divergence are given in Fig. 9 and above drag divergence in Fig. 10.

5.2. Section Lift-Drag Polars Obtained in Flight and Comparisons with Wind-Tunnel Results

The variations of profile drag coefficient with lift coefficient measured for three different test conditions on the rotor are shown in Fig. 11. In (a) the profiles are compared at a radius very near the blade tip and in (b) at a location approximately two chords from the tip. The polars in (c) are from tests in the same condition as (b) except that leading-edge roughness had been added to fix transition.

Within the limitations of the two-dimensional momentum analysis from which they were derived, and with certain qualifications inherent in the experimental method and discussed later, these polars provide a way of comparing the relative drag levels of the two profiles. In Fig. 11a the drag divergence at the higher values of lift coefficient is apparent for both profiles, the NACA profile having a slightly higher drag beyond this point. The same trend is apparent in (b), but the difference between the two profiles as shown here is not clearly defined beyond the drag divergence point, flight limitations preventing the necessary high values of lift coefficient being achieved. Some results from measurements taken at a slightly higher Mach number have also been included in (b) to provide extra data points for comparison although the difference in Mach number is not entirely insignificant. The outboard location shows a slightly earlier drag divergence in both cases. This is as expected on the grounds that the Mach number is higher but it is likely that the influence of the tip will also affect the strength of the shock, and hence the drag in this region. The third plot, Fig. 11c, shows the very significant difference that a small amount of surface roughness can make to the drag at these high values of lift coefficient near the stall. The drag rise occurs earlier and the difference between the two profiles is most noticeable as the penetration into drag-rise conditions is much greater.

Although the main purpose of this experiment was to compare the profile drag of each aerofoil at the same lift it is also of interest to compare absolute levels of drag with wind-tunnel results on a lift coefficient basis (Fig. 12). It should be noted that the tunnel tests were all conducted with leading edge roughness bands. Several differences are immediately apparent; in flight, drag divergence occurs at lower values of lift coefficient and after drag rise the difference in lift coefficient for a given value of drag is smaller than obtained during tunnel tests. Also the general level of drag in the transition-free flight tests is lower. Various factors which have a bearing on the interpretation of the results will now be discussed in some detail.

The high loadings on the gloved portion of the blades are associated with the incidences induced by the tip vortices of preceding blades. The spanwise distribution of induced incidence is affected by quite small translational velocities which exist even for carefully controlled 'hover' conditions. The resulting effect is a periodic incidence variation with azimuth at any spanwise station. These effects are discussed in more detail in Section 7 but they have repercussions when discussing the lift-drag polars because of the time-averaging process inherent in the test technique.

If the fluctuations of incidence occur at relatively low C_L values when both C_L and C_D vary linearly then the averaging process will produce points which lie on the lift-drag polar corresponding to steady conditions. If excursions of incidence enter into drag rise conditions the variation of C_D is non-linear and $dC_D/d\alpha$ increases with incidence, α, thus a higher value of C_D will be recorded for a given mean value of C_L. If however the incidence variation goes beyond the stall then the mean C_L will be lower than required for the corresponding value of C_D in static conditions giving a further displacement of the $C_D - C_L$ curve leftwards. The effect of periodic incidence fluctuation on the measured drag polar is therefore to make the initial drag rise earlier and reduce the apparent maximum lift coefficient obtainable. The extent of these effects depends on the magnitude of the fluctuations and time spent in the various domains of the polar. As each aerofoil on opposing blade tips is

subject to essentially the same incidence variations the difference in drag between the two profiles should be maintained and even accentuated if conditions exist in which due to a lower $C_{L_{max}}$ the NACA 0012 profile is stalled for a relatively longer period.

It has not been possible to construct an accurate estimation of actual incidence variation since the indication of incidence using leading-edge pressure difference across the stagnation point is not reliable near stall and beyond. However, the apparent early drag rise of the measured results attributable to this effect appears larger than expected. Additional support for this view is evident when the measured surface pressure distributions are compared with tunnel results on a C_L basis. Both profiles exhibit higher leading edge suction peaks and hence stronger upper surface shocks than the tunnel results at the same lift coefficient, substantiating the earlier drag rise. These differences are mainly associated with changes in surface pressure distribution occurring in the actual environment of the blade tip and will be discussed in detail in Section 6.

The generally lower level of drag up to the drag-rise point is to be expected for the transition-free flight results, as the tunnel tests were all conducted with leading edge roughness bands. Also the increase of Reynolds number by a factor of almost two, for the flight results, would further reduce the profile drag coefficients.

It was mentioned earlier that the measured difference in drag between the two profiles transition-free was less than expected and it was in this context that an apparent anomaly in surface pressure distribution of the NACA 0012 profile was investigated. It will be seen (Figs. 9 and 10) that the pressure difference between upper and lower surfaces of the NACA profile in the region of the trailing edge is noticeably greater than the RAE profile. The two profiles should be geometrically similar from approximately 30 per cent chord to the trailing edge and the thickening of the pressure distribution locally at the trailing edge is a typical effect of trailing edge camber.

On completion of the tests the geometric accuracy of both profiles was again checked. The waviness of the profiles (where it existed) was of the order of 0·3 mm. An anti-erosion strip was fitted to the nose of both test profiles extending rearwards 20 mm and 0·2 mm thick. It is considered that these discrepancies are relatively small in the context of the blade chord of 0·47 m. However, the trailing edge of the NACA profile was drooped by somewhat less than 1 mm resulting in positive camber over the last 70 mm of chord. Although this discrepancy is relatively small in terms of the blade chord it had a noticeable effect on the surface pressure distribution.

The effect of this distortion in profile was examined by calculating the change in pressure distribution with and without trailing-edge camber keeping leading-edge and trailing-edge points coincident. It was found that using the amount of camber actually present the lift coefficient was increased by 0·02 for a relatively small increase in peak suction (*i.e.* small compared with the increase in peak suction present if the incidence of the uncambered profile was increased to give a similar increase in lift coefficient). As will be discussed later the drag rise is largely dependent on the magnitude of the peak suction through the implied shock strength. The effect of trailing-edge camber on the NACA profile can therefore be expected to reduce the difference between the lift-drag polars of the two profiles. The relative difference between two specimen profiles could be more accurately represented by displacing the NACA points to the left by approximately 0·02 C_L.

A possible explanation of the relatively large difference in measured drag, at the highest values of C_L, when both profiles were roughened, is that the NACA profile was stalled whereas the RAE profile was not. This could also explain the lower values of C_L for the NACA profile but would seem to be a remarkably low C_L value for stall even allowing for averaging processes.

Bearing the above points in mind it will be seen from the results of the average pressure measurements there is a clear indication of the relative delay in the rise of profile drag coefficient for the RAE profile in the three-dimensional environment of the blade tips. However, there is some evidence that the difference is less marked at the spanwise station nearest the blade tip although the lift coefficients obtained were not in the event sufficiently high for complete confirmation. Compared with wind tunnel results, the drag rise appeared to occur earlier, partly due to genuinely higher peak suctions in the surface pressure distribution and partly to the effect of the averaging process involved in the measuring technique.

6. Surface Pressure Distributions and Resultant Forces

6.1. The Profiles compared in Flight

Surface pressure distributions for each profile shape were recorded in approximately 200 different combinations of flight state and measuring configuration. Although concentrating on the hover condition, sample records were made in translational flight and in transient manoeuvres. All the records made

contributed to demonstrating the consistency and accuracy of the measuring technique, and about half of them have been analysed further to provide the integral data used to compare the performance of the two profiles. Blade loadings from almost zero lift, up to conditions including transient stall have been produced by running the rotor through a wide range of collective pitch settings, from a 'ground run' at the lowest control setting, up to hovering at approximately 8000 ft altitude. Typical samples of these measurements were shown in Figs. 6, 7 and 8 and discussed with the profile drag results in Section 5.1. The top figure on each page shows the form of the plot used to evaluate the force parallel to the chordline and the centre figure, showing $C_p\sqrt{x/c}$ v. $\sqrt{x/c}$, was chosen to obtain the most accurate integral for the evaluation of lift and pitching moment.

A broader perspective of the difference between the two profiles in the rotor environment is provided by the mean surface pressures reproduced in Figs. 13 and 14. Each figure shows the pressures at four spanwise stations on each of the two gloves, the upper set in each case being for the new profile and the lower for NACA 0012. The results in Fig. 13 were obtained at low altitude and Fig. 14 at high altitude with the rotor consequently at a higher thrust coefficient and the local tip sections more deeply penetrating the development of local supersonic flow at the leading edge.

The relative differences between the two profiles are consistent and clear. For the corresponding (although not quite identical) conditions shown, the development of the local supersonic flow came later on the new profile, and less severely. The extent to which the principle of developing the lift with the minimum level of velocity on the upper surface has been realised can be demonstrated by examining the level of the pressures over the forward part of the upper surface (Fig. 15). The surface pressures at 1 and 5 per cent chord (covering the region at minimum pressure) indicate a lower level of local velocity on the new profile for all values of C_L; a difference which is maintained well beyond the sonic level, indicating that a reduced shock strength has been achieved.

It is useful to examine the local blade forces and moments in comparing the profiles with each other and also in the following sections of the Report where the flight results are compared with wind tunnel results and the three-dimensional aspects of the tip region are discussed more fully. As in two-dimensional test conditions the local section characteristics will depend on the local values of Mach number and Reynolds number, but in addition the local loads will depend on the three-dimensional flow conditions created by the rotor. For a given helicopter during hovering flight, the normal force coefficient C_N, chordwise force coefficient C_T (positive in the drag direction) and pitching moment coefficient C_m are functions of rotor thrust coefficient and the radial location, as well as M and Re, *i.e.*

$$C_L, C_T, C_m = f(t_c, r/R, Re, M_{tip}).$$

Rotor speed was adjusted during the flight tests to allow for temperature variations so that M was proportional to r/R, and since the effects of the small variations of Reynolds number encountered in these tests can be considered of secondary importance, the profile characteristics can be presented as functions of thrust coefficient and radial location. (Reynolds Number range is from $4{\cdot}5\times10^6$ to $6{\cdot}5\times10^6$.)

Fig. 16 presents measured values of C_L plotted in this way, with 16a giving the variation with thrust coefficient for constant r/R (and hence constant Mach number) and 16b giving the variation with r/R for constant thrust coefficient. Note that as the rotor thrust coefficient increases not only does the local incidence increase because an increasing collective pitch is applied to the rotor, but the local loading gradients change with the increasingly strong wake contraction. Thus the value of thrust coefficient, as well as the radial location, can determine the extent to which the local section loadings are sensitive to three-dimensional effects.

Clearly the measurements encompass the loading peak which occurs very near to the blade tip in the hovering condition and there is a suggestion that the peak becomes less sharp at the higher thrust coefficients. This may be due to the gradually increasing periods of transient stall which curtail the maximum values of C_L as the general level of loading is raised. A fuller description of the radial loading peak will be given when the unsteady pressures measured in this region are discussed. It should be noted that day to day variations between flights caused some scatter of the data beyond that which is inherent in the basic simultaneous measurements on which the comparison of the drags of the sections is made. Some of the scatter is thought to be associated with the remaining slight translational velocities which occur in notional hovering flight and the curves in Figs. 16, 17 and 18 are drawn with a knowledge of this scatter derived from wake measurements. This is possible since the wake measurements are repeated on every event, and as each of the four chordlines are measured in turn, it provides a useful check. The character of each set of four curves, and the essential compatibility of the cross-plotted curves also play a part in the choice of the 'best' smooth curve.

As mentioned previously the NACA profile was somewhat more highly loaded. This is almost certainly due to minor rigging differences between the two blades. Rigging adjustments showed the extreme sensitivity to

small changes of angle and the differences between the loading of the two test profiles is believed to be of this nature rather than any significant difference in the radial loading distributions.

The high values of C_L on the RAE(NPL) 9615 profile at $r/R = 0{\cdot}90$ for the three highest thrust coefficients, are not easily explained in terms of measuring errors, but they are unusual in that they do not conform to the loading trends shown by the rest of the results.

The corresponding values of chordwise force for this same range of conditions is shown in Fig. 17. Since shock-induced drag should be apparent as an increase in form drag, the normal pressure forces were resolved in the chord-wise direction as a step towards deriving the form drag of each profile shape. However, the main point revealed by these plots concerns the three-dimensionality of the flow near the blade tip and this will be discussed fully in Section 6.3.

Similarly, with the values of the pitching moment about the quarter-chord position (Fig. 18), the main feature of the plots is the way in which the pitching moment varies in a spanwise direction. Generally the cambered profile, RAE(NPL) 9615, shows a nose-down increment of pitching moment coefficient relative to the symmetrical section of approximately 0·005, but even this relative level is changed at the extreme blade tip.

6.2. Comparison of Flight and Wind-Tunnel Surface Pressure Distributions

The mean pressure scanning system produced consistent pressure distributions closely resembling the shapes of those for the two-dimensional aerofoil through the whole incidence range. The incidences of greatest interest are those where local supersonic flow develops over the first 10 to 20 per cent of the upper surface leading to the ultimate breakdown of the flow. These conditions were present near the tip for all hover conditions, and occurred with increasing severity as altitude increased.

The gradual development of the supercritical flow and the onset of flow breakdown is shown in Fig. 19 by the progression of loadings derived from steady two-dimensional wind tunnel tests[1]. A detailed interpretation of the type of stall shown by both profiles was presented in Ref. 8. This emphasised how, for such conditions on this type of aerofoil, the stalling process involves an interaction between (1) a shock-induced separation which is provoked at the leading edge as the local supersonic flow develops with incidence and (2) a subsonic-type, rear separation which has already been growing from the trailing edge. The shock-induced separation, by thickening the upstream boundary layer, accelerates the growth of the rear separation and at a critical point of 'bubble burst', triggers a sudden forward jump of the rear separation; the two separated flows link in this process. As the stalling continues the local supersonic flow at the leading edge collapses. The tunnel results in Fig. 19 illustrate this development. For the NACA 0012 profile, the bulge B in the pressure distribution for 7 deg incidence indicates the characteristic bubble growth for a localised shock-induced separation. The manner in which this increases the severity of the rear separation is indicated by the increasing amount by which the pressures near the trailing edge depart from the low incidence values, *i.e.* by the divergence of trailing edge pressure. This is just about detectable at R for 7 deg and is quite pronounced by 8 deg. By this latter stage too, the stalling process has begun in which the local supersonic flow collapses under the influence of the interacting shock-induced and rear separations.

There is quite a striking similarity between the broad impression created by Fig. 19 and that created by Figs. 13 and 14 which compare the mean pressures on the two profiles on the tips of the *Wessex* rotor in flight. This similarity applies both to the general shape of the pressure distributions with their local regions of supersonic flow and quite evident shock waves and, especially important, as has already been noted, to the relative properties of the two profiles. The similarity is all the more striking when the unsteady nature of the flow, caused by the periodic movement of the tip vortices, is appreciated. These effects of vortex interaction are described in detail in Section 7 and include significant radial variations in both Mach number and incidence and also strong cyclic variations in incidence which in the extreme cases involved dynamic excursions into and out of stall. The profiles evidently responded to these complex changes qualitatively in the same relative way as they did in the steady aerofoil tests.

6.3. Blade Tip Effects

Having established the broad similarity between pressure distributions measured in flight and in a wind tunnel, there are also significant differences, consistent with the higher drag measurements obtained in flight. The nature of these differences is generally a progressive departure from the tunnel measurements as the blade tip is approached.

Fig. 20 shows a sample pressure distribution for each profile superimposed on the two-dimensional pressure distribution at the same lift coefficient and Mach number. There was only limited scope for direct comparisons because of the difficulty of precise interpolation between the values of Mach number and incidence available from the tunnel tests. These two examples were measured simultaneously in flight at 6000 ft altitude, and are for a measuring station very close to the tip ($r/R = 0{\cdot}964$) which is only 1/3 chord from the end of the parallel portion of the planform and only 2/3 chord from the extreme tip. Three-dimensional effects would certainly be expected to influence the performance of the profile in this region and it is perhaps surprising that such a high loading was still generated. It can be seen that each profile has a lower level of minimum pressure than is found in wind tunnel results for the same lift coefficient, and a correspondingly greater shock strength. This is presumably a further reason (as well as the effects of the unsteady loading on the mean measurements) for the higher drag that is found in the flight results.

The trend towards lower levels of minimum pressure for a given lift coefficient can be demonstrated by comparing the values of upper surface pressure at 0·01 chord as measured in flight and wind tunnel, for a range of local lift coefficients, at different radial stations. Fig. 21 shows the immediate outboard station (a) in contrast with the extreme inboard station (b); the generally lower levels of pressure at all lift coefficients is evident in the flight measurements, but closer agreement between flight and tunnel results occurs at the measuring station furthest from the blade tip.

The other immediately obvious difference between the flight and the tunnel results (Fig. 20) is the higher level of pressure (or reduced suction) over the remainder of the profile for the flight case. The upper surface pressures at 0·5 chord, taken as a representative sample of the rear part of the upper surface pressure distribution, become progressively higher than the tunnel results as the blade tip is approached. They are compared at the extreme inboard and outboard (nearest the tip) chordlines in Fig. 22. Thus the sample pressures at 0·01 chord and 0·5 chord, when compared with two-dimensional results at the same lift coefficient, clearly illustrate the forward shift of the loading on the aerofoil in the tip region. (Since surface pressure is dependent on Mach number the effect of errors in the measurement of the velocity of the incident airstream on the rotor must be carefully considered. However, examination of the trends shown by the wind tunnel results indicates that improbably large errors of Mach number would be necessary to explain the differences apparent in the tip region.)

Returning to the pressure distributions presented in Fig. 20, it is seen that it is not only the upper surface pressures but also the lower surface pressures that are greater than the two-dimensional results and this suggests a reduction in effective thickness of the blade section. On closer examination however it is seen that the differences in lower surface pressure over the rear of the profile are less than the differences in upper surface pressure so that there is still a loss of lift over the rear of the aerofoil compared with the two-dimensional results. Both the reduced thickness effect and the forward shift of the loading are well known features of tip effects in fixed wing aerodynamics, where the latter is attributable to the influence of the varying downwash field. In this respect, the surface loading distribution in the tip region resembles that on a low aspect ratio twisted (washed-out) wing of rectangular planform. The significance of this departure from the pressure distributions on corresponding two-dimensional aerofoils is clearly shown by the values of the local force and moment coefficients in the tip region. The variations of C_L, C_T and C_m with radial position on the blade and with rotor thrust coefficient are shown in Figs. 16, 17 and 18.

The forward shift of the centre of pressure shows in the comparison of the flight and two-dimensional values of the pitching moment coefficients. For two-dimensional test conditions the NACA 0012 profile will have a nominally zero pitching moment and the RAE(NPL) 9615 profile a small nose-down pitching moment due to its slight camber ($C_m = -0{\cdot}01$ at zero incidence). The flight measurements in Fig. 18a show that for each spanwise station there is a gradual increase in pitching moment with rotor thrust coefficient, corresponding to the progressively further inboard location of the adjacent vortex. At 0·9 radius the pitching moments almost correspond to the two-dimensional values, but the significant differences between the flight and tunnel results are more easily seen in Fig. 18b; there is a large increase in the level of pitching moment for both profiles as the tip is approached. This is clearly a result of the changes in chordwise loading distribution apparent in Fig. 20.

The pitching moments have shown a departure from two-dimensional section characteristics in the tip region, but the chordwise force coefficients derived from the integrated normal pressure forces demonstrate the three-dimensional behaviour of the aerofoil in the tip region in a more fundamental way. When calculating the performance of the highly loaded tip region of the rotor blade, the usual 'lifting line' assumption, that the downwash induced by the streamwise vortices does not vary along the chordline, is not valid since there are large changes of blade loading over only a few chords' length of the rotor radius. Thus the use of two-dimensional section data (in the calculation of blade forces and moments) in the tip region will not give the true result. In Ref. 9 it has been shown that for finite wings of low aspect ratio (on which the load distribution

resembles that on the tip region of the rotor blade) the concept of an 'effective incidence' is still valid, but that the sectional lift slope is reduced from the value appropriate to a two-dimensional aerofoil.

The extent of this departure from two-dimensional section characteristics in the blade tip region can be shown by deriving the 'effective sectional lift slope' from the locally measured forces normal to and along the blade chordline. For an idealised aerofoil in inviscid flow, if α_0 is the zero lift angle and α_e the effective incidence, then

$$C_N = a(\alpha_e - \alpha_0) \qquad \text{and} \qquad \alpha_e = -\frac{C_T}{C_N}$$

so that

$$a = -\frac{C_N^2}{C_T} \Big/ \left(1 - \frac{\alpha_0}{\alpha_e}\right)$$

showing how the sectional lift slope, a, is related to C_N^2/C_T.

The presence of the small term containing the zero lift angle α_0 means that $-C_N^2/C_T$ is not quite identical to the sectional lift slope for the slightly cambered section, RAE(NPL) 9615. Nevertheless, a comparison with the corresponding two-dimensional results similarly derived by integration of the normal pressure forces can provide a useful indication of the departure from two-dimensional section characteristics in terms of a quantity which can be closely associated with the sectional lift slope. It is important to remember that only sectional characteristics are being examined in this analysis. The angle of the local incident stream relative to the direction of motion of the blade is not involved, so that the induced drag does not affect the values of C_N^2/C_T measured.

Values of C_N^2/C_T have been derived from curves fitted through the measurements of C_L and C_T in Figs. 16 and 17, taking C_L equal to C_N. In Fig. 23 values of C_N^2/C_T are shown as a function of the spanwise (radial) position along the blade for each blade profile. Measurements are shown for four values of the rotor thrust coefficient and for each case the values of C_N^2/C_T derived from two-dimensional wind tunnel pressure measurements at corresponding Mach numbers and lift coefficients are shown for comparison. These curves show that towards the blade tip C_N^2/C_T has smaller negative values than the two-dimensional results indicating a considerable reduction in the sectional lift slope. Here we have a suggestion of the strong three-dimensional effects that are known to be found in the region of the tip of a fixed wing aircraft. (The displacement of the curves for the RAE(NPL) 9615 profile from the NACA 0012 results is attributable to the camber of the former, both for the flight and tunnel results.)

However, the measured values of the chordwise force will include a contribution from form drag (arising from viscous effects). Clearly for an aerofoil in viscous flow, the form drag will tilt back the direction of the resultant force on the aerofoil, giving larger negative values of C_N^2/C_T. For the range of incidence relevant to these measurements the two-dimensional results are quite uniformly displaced to slightly more negative values, (*e.g.* $-\frac{C_N^2}{C_T} = 10$ whereas the two-dimensional lift slope is 7·2 at $M = 0{\cdot}6$).

For the rotor blade tip both the change in effective thickness and the lift-dependent chordwise redistribution of lift will tend to increase the strength of the upper surface shock, for a given lift coefficient. Thus the profile drag will be increased and this increase is substantiated by the wake measurements of profile drag. Since the shock-induced drag rise is almost entirely felt as an increase in the form drag of the profile, the earlier drag divergence will be reflected in the values of C_N^2/C_T and will offset to some extent the changes due to the reduced sectional lift slope. Fig. 23 can thus be taken to indicate that there is a significant departure from two-dimensional section characteristics over most of the highly loaded tip region of the rotor blade in hovering flight, the reduction in effective sectional lift slope being revealed by the smaller negative values of C_N^2/C_T, despite the masking effect that the earlier drag divergence has on these values.

Some comment on the overall accuracy of the measurements is appropriate, since comparisons have been made on an absolute basis, between sets of measurements obtained in entirely different test conditions (*i.e.* two-dimensional steady wind-tunnel tests at a reduced Reynolds number have been compared with in-flight measurements on the tip of a rotor blade). It should be remembered that the essential feature of the flight experiments is the ability to make simultaneous comparisons of the two profiles in the same test conditions. Nevertheless careful analysis of the rotational effects on the pressures transmitted to the rotor hub, and on the recording system gives some confidence that the absolute values can provide useful comparisons, not only

when considered singly, but when observed as progressive changes, spanwise along the blade, and for gradually increasing rotor thrust coefficients. In particular, it is important that comparisons with wind-tunnel results are made at the same Mach number. For the flight tests, as previously discussed, the velocity of the oncoming stream was taken to be the product of the rotational speed and the local radius. The swirl induced by the rotor, as predicted by a simplified theoretical model, is very small indeed, and the viscous wake of the other blades is assumed to lie in the rolled-up vortex sheet clear of the test blades, below the plane of the rotor. Evidence from the measured pressure time histories discussed in the next section supports this assumption (based on information from model tests) that the tip vortex from the previous blade lies clear of the measuring blade. There is some indication that for certain near-hover flight conditions the rapidly fluctuating pressure traces produced at an azimuth position near the tail rotor may indicate the fringe of the vortex approaching the test section, but these conditions were not present in the majority of recorded events, and they are not thought to affect the analysis significantly.

In conclusion it can be said that the measurements of the surface pressure distribution confirm the difference in drag between the two profiles detected by the wake measurements using pitot tube rakes. Characteristic features are present which show that the section performance limits were dependent on the same flow phenomena that were present in the wind tunnel tests. However, the levels of minimum pressure on the upper surface were consistently lower than those from two-dimensional tests at the same lift coefficient and this difference was greatest near the blade tip. The increase in relative velocity with radius and the non-uniform inflow velocity combine to produce such high loadings in the tip region that the tip effects which are normally negligible on a high aspect ratio planform become of the greatest significance. The collected force and moment data have shown that the changes illustrated by the sample pressure distributions chosen for discussion are effects of real significance over the whole of the region of the radial loading peak. They will reduce the value of the maximum lift coefficient available, increase the drag of the profile and produce undesirable pitching moments. From the flight results, lacking an accurate measurement of the incidence distribution, a full analysis of the local section characteristics is not feasible. The separate lift and thickness dependent changes appear to be in reasonable agreement with simple theoretical predictions of the effective thickness-chord ratio and the change in chordwise load distribution near the tip. These measurements suggest that accurate lifting surface calculations could usefully be employed to improve the design of rotor blade tips in the region inboard of that affected by the extreme tip edge vortex, and incorporating the whole of the region which is highly loaded in hovering flight. In addition to the changes of planform twist and thickness usually considered, this may lead to a graded increase in positive camber in the tip region, for an optimised blade design.

7. Unsteady Pressure Measurements

7.1. The Nature of the Variation of Local Incidence with Azimuth

During the development of the gloves and their instrumentation, the opportunity arose to incorporate in the RAE(NPL) 9615 test profile four miniature pressure sensors to monitor instantaneous pressures at selected chordwise positions. The intention was to evaluate these types of sensors and their mounting techniques on the blade, for more extensive measurements of instantaneous pressure planned for future flight tests, and to investigate possible means of indicating local aerodynamic incidence and flow separation. As an indication of incidence a transducer was set to measure the difference in pressure between 1 per cent chord on the upper surface and 5 per cent chord on the lower surface. This difference was known in two-dimensional wind-tunnel tests to increase monotonically, up to the stall, with incidence. An early sign of stall is the onset of boundary-layer separation at the trailing edge and is indicated by the divergence of trailing-edge pressure. It was to detect the latter that a transducer was positioned to measure the pressure difference between upper and lower surfaces at 94 per cent chord. In the event, the pressure time-histories recorded by these transducers have helped in several ways, but a simple conceptual model of the near wake, describing the tip vortex locations, was required to explain some of the fluctuating pressure records that were obtained in supposedly steady conditions.

The high angles of incidence induced by the tip vortices of preceding blades contribute to the high loadings found near the tip of each blade, and the measuring stations on the blade glove were intended to encompass the resulting peak in the spanwise loading. Fig. 24 shows that this was realized, and compares the measured loadings with predicted values[11] and the measurements of Sheiman[10] for the same thrust coefficient. The very high loading peak and, of even more importance in the present context, the high adjacent loading gradients, are immediately evident.

The strong loading gradients result from the rapid spanwise variation of induced incidence and indicate that large variations of loading can occur at a given spanwise station as a consequence of small lateral displacements of the tip vortex system. Simple considerations indicate that the vortex wake can be significantly skewed by quite small translational velocities of the helicopter relative to the air, which are inevitable even for carefully controlled hover conditions. (In fact, for a small range of translational velocities near the hover, there are indications that the vortex sheet rolling-up process will amplify the initial skewness of the wake. This process is incorporated in the simple wake model discussed in this section.) The associated distortion of the tip vortex patterns relative to the rotor hub, results in a harmonic variation of induced incidence at each measuring station during every revolution of the rotor. The locus of the points of intersection (in plan view) of a blade and the tip vortex of the preceding blade during one revolution is a circle, whose centre is displaced downwind from the centre of the rotor, and whose radius is less than the rotor radius (Fig. 25). The entire pattern of vortex-induced downwash velocities will oscillate, relative to a given measuring station, in a spanwise direction, giving rise to the characteristic variation of incidence shown at the bottom of Fig. 25. The development of the unsteadiness with increasing translational velocity can be predicted, and the flight tests consistently produced broadly similar results. A typical example of the incidence increments produced by the tip vortex of the previous blade over the whole tip region is shown in Fig. 26, for a forward speed of 5 kn. The spanwise extent of the relatively large incidence fluctuations is seen to be very limited; they are in fact greatest in the region of the present measurements.

The prediction of the local blade-loading variation for increasing forward speeds with this simple model raises several interesting points. As the translational velocity increases, the harmonic radial displacements of the loading peak increase in amplitude, but at some point the normal mechanism governing the graduation of the loading to zero at the blade tip will prevent the full loading peak being generated at the azimuth position where it approaches the tip. The strength of the vortex trailing from the tip of each blade will be diminished at this azimuth position, which in turn will further reduce the value of the loading peak. Variations of the strength of the trailing vortex around the azimuth are not represented in the simple model.

Nevertheless, the real course of events with increasing translational speed can be described qualitatively provided the effects of the changing strength of the tip vortex are anticipated. For small velocities there will be a slight asymmetry in the two loading peaks characteristic of this radial location corresponding to the difference in strength of the trailing vortex on the advancing and retreating blades. This is apparent in the measured incidence cycles. As speed is further increased a large transient decrease in the peak blade loading will begin to appear at $\psi = 0$ (the back of the rotor disc) as the vortex approaches the blade tip. This change occurs rapidly over a small forward speed range, and will give rise to a large increase in vibration level and a significant trim change, due to the change in overall blade loading. The wake model provides a new insight to this region of 'translational buffet' in the helicopter's flight envelope. The measured time-histories at several positions along the blade may be used to deduce the vortex location compatible with their shape and phase, so providing a useful check on the wake geometry.

The instantaneous pressures near the leading edge reflected the variations of incidence due to the vortex velocity field (Figs. 28 and 29) and indicated that they were indeed quite large. (Similar pressure time-histories were recorded by Sheiman[10] for so-called hovering flight.) The absolute scale of incidence should be treated with some caution; it has been derived from a calibration obtained in steady wind-tunnel aerofoil tests, is applicable only up to the stall, and may not hold during blade-vortex interactions or near the blade tip. The mean pressure measurements show clearly that there were slight changes in the nature of the surface pressure distributions near the extreme blade tip and these inevitably affect the incidence calibration obtained from two-dimensional tests. Nevertheless, the incidence calibration is an adequate guide to the range of incidence in a typical cyclic variation, and the range of approximately 5 to 10 degrees is highly significant in relation to that over which the local supersonic flow develops. Depending on the level of the mean values, the periodic variations are likely to take the local flow into and out of regions of supersonic velocity and drag rise and even into and out of shock-induced stall.

Having established the mechanism of the type of unsteadiness to which the blades were exposed in the near-hover and found that it has strong three-dimensional features which distinguish it from oscillatory aerofoil loadings commonly investigated for rotor aerofoils (*i.e.* retreating blade stall and stall flutter) it is of interest to find where the limits to the effectiveness of the profiles lie and the mechanism of the flow separation and re-attachment in these transient loadings.

At the onset of rear separation the pressure differences between the two surfaces at 0·94 chord begins to rise steeply (trailing edge pressure divergence)[8] (Fig. 27). The cycle of incidence variations caused by the changing vortex location gives two incidence peaks per revolution of the rotor, so that typical samples of trailing-edge pressure difference show two characteristic spikes as the flow separates transiently (Figs. 28a and 29a). The

leading edge pressure difference, measured between 0·01 chord on the upper surface, and 0·05 chord on the lower surface follows the characteristic 'double hump' shape of the incidence variation, but it must be remembered that at the stall, the leading edge suction collapses and so the maximum value of leading edge pressure difference is not necessarily a measure of the maximum incidence reached in the excursion. Indeed, for the example in Fig. 29a there is a clear suggestion that the stall increased in severity well beyond the stage at which the maximum leading-edge pressure difference was reached.

Each flight state recorded produced a trace showing approximately 50 rotor revolutions. Generally the same shape of trace was maintained for each revolution during the whole of the event provided no inadvertent change in the trim of the helicopter occurred. There were slight random cycle-to-cycle variations but these were insufficient in magnitude to alter the basic shape and were probably associated with the transient flow separations encountered on the blades. The effects of the small random cycle-to-cycle variations were eliminated by taking average values for a large number of cycles in each event. (Atmospheric turbulence near the ground on windy days and flight in ground effect produced traces with a very much larger random variation, making any further analysis of little value.) Analysis of a series of progressively more severe blade loadings (Fig. 27) shows that the trailing-edge pressure divergence appears for conditions in which the peak incidence (or leading-edge pressure difference) exceeds a certain critical value. As might be expected, this critical value is higher for the transition-free results than for the transition-fixed ones. Beyond the onset of this divergence, for each of the two boundary-layer conditions, the magnitude of the maximum excursions in trailing-edge pressure correlates reasonably well with the maximum value of the peak in leading-edge pressure difference.

The correlation with stall onset in the steady wind-tunnel aerofoil tests is within 1 degree of incidence. This is surprisingly good in view of the three-dimensionality and time dependence of the flight environment. It is of the same order, for example, as the difference between transition-free and transition-fixed conditions in flight. It is clear however that in flight, as in the tunnel experiments, the onset of stall is dependent on the degree of surface roughness and most of the flight tests were made without roughness bands. For these the presence of significant regions of laminar flow was accidentally revealed by deposition of a sooty film from atmospheric pollution in areas of turbulent flow. The transition line was irregular, with turbulent wedges growing from minor surface irregularities and aligned in a chordwise direction indicating that cross-flows in the boundary layer were small or non-existent. In some areas laminar flow persisted for up to 0·40 chord. For the wind-tunnel conditions roughness bands were chosen to give a turbulent boundary layer at the shock for a range of test conditions. Corresponding scale roughness was employed in flight, but a somewhat denser covering of carborundum particles was applied, so that the boundary layer may have been unnecessarily thickened.

7.2. Hysteresis of Trailing-Edge Separation with Incidence (Stall Hysteresis)

The leading-edge and trailing-edge pressure differences have been used as indicators in attempting to analyse the dynamic stall development. By correlating these two measured pressures through one complete incidence cycle, *i.e.* one rotor revolution, some features of the flow at the onset of, and recovery from, the stall can be inferred.

Fig. 28 has been chosen to illustrate a typical incidence cycle with small excursions into regions of breakdown of the flow around the aerofoil. Part (a) shows a plot of the leading edge pressure difference against azimuth, and part (b) the trailing edge pressure difference. By contrast, Fig. 29 is a sample with a higher mean loading and having a leading edge roughness band, so bringing forward the onset of separation as shown in Fig. 27. A much more extensive breakdown of the flow occurs during these cycles. The transition free sample in Fig. 28 is typical of the traces recorded for conditions where the mean measurements of lift and drag were near the region of 'drag divergence', *i.e.* where the drag polar starts to rise steeply. The incidence cycle seems to take the profile to a point of incipient stall (point B). In contrast to this the transition fixed case (Fig. 29) corresponds to a condition well into the high mean drag state ($C_{D_0} = 0{\cdot}02$) and although it is reasonable to assume that the same characteristic 'double-humped' incidence cycle is occurring, clearly the leading-edge suction peak is breaking down transiently (point Q) so that the aerofoil can be considered to have been partly stalled for a portion of each cycle. Although the leading-edge pressure peak Q is only very slightly higher than P, the trailing-edge pressure is very much higher at G, suggesting that incidence is much higher than indicated by the leading-edge pressures.

Following through the concept of the dependence of flow separation on shock strength shown by the tunnel results and confirmed by the statistical analysis of the flight results (Fig. 27), the values of leading-edge pressure difference and trailing-edge pressure difference are shown plotted against one another in Figs. 28c and 29c. The transition free example shows a series of narrow loops along the general line of the curve derived

from the peaks analysis in Fig. 27, giving little trace of any hysteresis. However, the second example which penetrates further into the stall shows a marked degree of hysteresis. Here the flow separation and re-attachment proceeds as follows. Starting from a relatively low value at point 0, the incidence rises and falls through two successive peaks P and Q (the second larger than the first due to the lateral asymmetry of the rotor wake) during which the data plot of Fig. 29c describes two successive loops (in an anti-clockwise sense) of similar shape. Both loops start with a divergence from the base line as the value of leading-edge pressure difference exceeds the value, about 0·45, that is critical for the transition-fixed conditions (see Fig. 27). It can reasonably be inferred that the severity of the separation is increasing progressively as the trailing-edge pressure difference continues to rise. The leading edge-pressure difference at first continues to increase; this implies that the incidence was at first continuing to increase. It is also reasonable to assume that incidence was still increasing round, and to some point beyond, the stationary value in leading-edge pressure difference; this is because wind-tunnel results for this profile have shown that the leading-edge supersonic velocities begin to collapse as incidence increases into stall for these Mach numbers.

It can be deduced however that incidence almost certainly began to decrease at some point on the loop before the apex was reached. This is because the value of the leading-edge pressure difference at which the line falls sharply from the apex of the loop to the base line corresponds to a significantly lower incidence than is implied by the maximum value of this difference (at least $1\frac{1}{2}$ degree lower for loop Q). What cannot be deduced is just where incidence began to fall.

It is clear that attached flow has been re-established at both leading edge and trailing edge by this stage. It is of some interest to note that the velocity at the upper-surface leading-edge hole that was being used for this exploration remained supersonic for the whole of the first loop P, but for the second loop Q had fallen to a value just below sonic before re-attachment occurred. (Sonic velocity corresponds to a value of the leading-edge pressure difference of about 0·4.)

The flow conditions existing at each point around these loops might thus be explained qualitatively in terms of the known features of the performance of a two-dimensional aerofoil. However, the simple line-vortex model (Fig. 25) describing the essential three-dimensionality of the overall flow geometry suggests that the separated regions of the flow may be radically different to that on a stalled two-dimensional aerofoil having the same section. For the conditions where the loading peak includes a stalled region (Fig. 29) the passage of this local separation over the measuring station, following the radial oscillations of the vortex location, may give rise to separation and re-attachment conditions which differ from the two-dimensionally-derived criteria. The pressure time-histories show a cross section of the stalled region as it passes the measuring point and the features of the edges of this separated region must be influenced by the crossflows generated by the steep loading gradient. Clearly these three-dimensional effects combine with the unsteady features of the flow to produce the particular type of time-dependent flow phenomena observed on the rotor.

The question arises, are the time-average comparisons made between the characteristics of the two profiles in flight critically dependent on the precise shape of the incidence cycle to which they were subjected? Several tests were made during which translational and vertical velocities of varying degree were introduced in 'hovering' flight. The character of the pressure time-histories was considerably modified by the changes in wake geometry so caused. Relatively large departures from hovering flight, typically 20 kn translational speed or 100 ft/min vertical velocity, produced mean loadings which for some directions of flight were less than the loads in hovering flight, but other combinations of vertical and translational velocity produced mean loadings higher than could be attained whilst hovering. These results provided useful additional comparisons of the two profiles, but of greater importance, they showed that the relative behaviour of the two profiles, deduced from the mean pressure measurements, was maintained for a variety of loading patterns. However, the inadvertent departures from hovering flight were always considerably smaller than these deliberate excursions and examination of a large number of traces showed that the scatter of the hovering results was not attributable to the minor changes in the character of the incidence cycle from one flight to the next.

The instantaneous pressure measurements made on the RAE(NPL) 9615 aerofoil during these experiments are sufficient to provide some link with the oscillatory aerofoil experiments performed during the wind-tunnel development of this profile and to make some reference to the background of information on oscillatory aerofoil performance. The dynamic stability boundaries were investigated by a free oscillation technique[12] and in some more recent work at RAE unsteady surface pressure distributions have been measured on an oscillating aerofoil. From these results it can be deduced that the same basic nature of the stall is retained in steady and oscillatory aerofoil tests and in flight; the sudden, leading-edge triggered, 'blow-up' of an already developing rear separation is present in all three cases. The concept of trailing-edge pressure divergence can be carried over to oscillatory flow and for this type of stall it will indicate clearly the critical stage in its development. The effect of leading-edge roughness, which in the flight measurements can be clearly seen to

limit the maximum level of leading-edge suction developed (Fig. 27), tie in well with stall-flutter tests where leading-edge carborundum bands caused the areas of negative damping to be extended considerably.

The rates of change of incidence in the flight tests were relatively small and for these Mach numbers (0·55 to 0·6) negligible 'dynamic overshoot' of lift coefficient is predicted by oscillatory aerofoil tests[13]. This is confirmed by the flight results but stall hysteresis is a more difficult point on which to make close comparisons. The degree of hysteresis will be critically dependent on the type of stall experienced, which in turn will be a function of the exact profile shape. The three-dimensional conditions on the rotor which give rise to the oscillatory 'stall cell' phenomena add a further complication. The present measurements were sufficient to demonstrate a significant degree of hysteresis locally, but a fuller explanation must await the results of the more extensive pressure survey now in preparation: results which, if they are to provide the essential three-dimensional plus unsteady combination, can only be obtained from rotor testing.

The value of the pressure time-histories can be appreciated when it is remembered that the aerofoils encounter an incidence range up to and beyond the normal performance limits in each revolution of the rotor in the near-hovering case. Thus the location of these limits and the nature of the flow phenomena governing them in the actual environment can be found from a full analysis of each cycle.

Operationally, near-hovering flight with respect to the air mass is more common than 'classical' hovering. The near-hover provides an extremely useful test-case in which unsteady blade-vortex interaction may be studied but in addition it is an operationally important design case for the rotor, for if the blade tip region is to be refined for improved performance in the highly-loaded hover configuration, then the unsteady aspects of the environment are a real design consideration. Any detailed understanding of the noise generated by the rotor also demands a knowledge of these unsteady loads in the commonly encountered near-hover flight case.

8. Conclusions

The performance of two different aerofoil profiles, NACA 0012 and RAE(NPL) 9615 have been compared in hovering flight. The aerofoils took the form of fairings or 'gloves' at the tips of opposing blades and both local surface pressure and local wake pitot pressure measurements were made. The RAE(NPL) 9615 profile was designed, and expected on the evidence of two-dimensional tunnel tests, to give an all-round improvement in performance: to the shock-induced limits on the advancing blade, to the retreating blade thrust limits and to the loading that could be sustained without shock-wave drag in hover. It is the latter feature which has been investigated experimentally and reported here: the key issue being the behaviour of the profile in the three-dimensional environment of the blade tip.

The tests have allowed comparisons to be made between the two profiles in terms of lift-drag polars and details in surface pressure distribution. Comparisons with respective two-dimensional wind-tunnel test data have also been made. The effects of blade-vortex interaction on the blade loading were pronounced both in terms of spanwise loading and in periodic changes of local incidence, and the analysis has given some insight on various flow phenomena in the tip regions. It is also hoped that these measurements may provide a basis for comparison with theoretical prediction methods appropriate for the unsteady transonic region near the blade tip. The principal findings are listed below.

(1) The critical drag rise of the RAE(NPL) 9615 aerofoil occurred at a higher lift coefficient than that of the NACA 0012 but by a smaller margin than demonstrated in wind-tunnel tests. The difference between the two sections was particularly noticeable with roughened blades, which allowed a deeper penetration into drag-rise conditions during these tests.

(2) Consistent with the reduced profile drag of the RAE profile at higher lift coefficients, the measured upper-surface peak suctions were relatively smaller.

(3) The rise in profile drag of both sections occurs at lower values of lift coefficient than indicated from tunnel tests. This is largely attributable to the higher peak suctions in the three-dimensional flow, but some of the difference is inherent in the averaging process during measurement.

(4) The essential features of the surface pressure distributions present in the two-dimensional tunnel results were evident in the flight test results. However the peak suctions of both profiles were generally higher than those measured in the tunnel. This characteristic is consistent with the general increase in profile drag recorded in flight and mentioned above.

(5) The flight and tunnel surface pressure distributions were most similar at the inboard position, but as the tip was approached there was a progressive change in the pressure distribution characterised by an increase in forward loading in the flight case.

(6) The increased forward loading of the flight results suggest that performance in hovering could be improved by incorporating increased positive camber of the profile, applied progressively towards the tip.

(7) The effects of blade-vortex interactions were pronounced both in terms of spanwise loading distribution (at the test section the blade loading was virtually doubled) and in terms of periodic changes in local incidence due to distortion of vortex paths in the presence of quite small translational velocities of the aircraft.
(8) Miniature pressure transducers measuring instantaneous differential pressures between upper and lower surfaces near the leading edge and trailing edge of the blade were extremely useful in defining local 'incidence' and 'stall' respectively. The agreement with tunnel data on these simple criteria was encouraging.
(9) The local incidence variations, for small translational velocities, are caused by the oscillating flow pattern of the trailing vortex system. The response of the RAE profile showed a stall hysteresis which is likely to be of a time-dependent nature, but the three-dimensional aspects of this flow imply that the details of this separation and re-attachment may differ from those measured in two-dimensional oscillatory tests.

LIST OF SYMBOLS

a	Sectional lift slope
b	Number of blades
c	Blade chord
$\bar{C}_{D_0}$	Profile drag coefficient
$\bar{C}_L$	Mean lift coefficient
C_T	Chordwise force coefficient (positive in drag direction)
C_m	Pitching moment coefficient about quarter-chord
C_p	Pressure coefficient
H_0	Ambient total pressure (relative to local blade section)
M	Mach number
M_{tip}	Blade tip Mach number
p, p_0	Local and ambient values of static pressure
p_r	Pressure at radius r
p_{root}	Pressure at blade root
r	Radius of measuring point
R	Blade radius
Re	Reynolds number
$t_c = \dfrac{\text{thrust}}{\rho bcR(\Omega R)^2}$	Rotor thrust coefficient
T, T_0	Local and ambient values of temperature
x	Coordinate along chordline
z	Coordinate normal to chordline
α	Section incidence
α_e	Effective incidence
α_0	Zero-lift angle
ρ, ρ_0	Local and ambient values of density
ψ	Blade azimuth angle
Ω	Rotor speed

REFERENCES

No.	*Author(s)*	*Title, etc.*
1	N. Gregory and P. G. Wilby	RAE(NPL) 9615 and NACA 0012—A comparison of aerodynamic data. A.R.C. C.P. 1261. 1968.
2	H. H. Pearcey, P. G. Wilby, M. J. Riley and P. Brotherhood	The derivation and verification of a new rotor profile on the basis of flow phenomena; aerofoil research and flight tests. AGARD meeting. The aerodynamics of rotary wings. Marseilles. 1972.
3	W. J. McCroskey	Measurements of boundary layer transition, separation and streamline direction on rotating blades. NASA TN D-6321. 1971.
4	E. C. Maskell	Progress towards a method for the measurement of the components of the drag of a wing of finite span. R.A.E. Technical Report 72232. 1973.
5	A. J. Landgrebe	The wake geometry of a hovering helicopter rotor and its influence on rotor performance. American Helicopter Society 28th Annual National Forum. 1972.
6	T. A. Cook	Measurements of the boundary layer and wake of two aerofoil sections at high Reynolds numbers and high-subsonic Mach numbers. A.R.C. R. & M. 3722. 1971.
7	J. S. Thompson	A simple method of computing C_D from wake traverses at high-subsonic speeds. A.R.C. R. & M. 2914. 1944.
8	J. Osborne and H. H. Pearcey	A type of stall with leading edge transonic flow and rear separation. AGARD CP No. 83, Göttingen. 1971.
9	D. Küchemann	A simple method for calculating the span and chordwise loading on straight and swept wings of any given aspect ratio at subsonic speeds. A.R.C. R. & M. 2935. 1956.
10	J. Sheiman	A tabulation of helicopter rotor-blade differential pressures, stresses and motions as measured in flight. NASA TM X-952. 1964.
11	C. V. Cook	Rotor performance prediction in hover. Westland Helicopters Ltd., Research Paper 357. 1968.
12	A. W. Moore, N. C. Lambourne and L. Woodgate	Comparison between dynamic stability boundaries for NPL 9615 and NACA 0012 aerofoils pitching about the quarter-chord. A.R.C. C.P. 1279. 1971.

APPENDIX A

Radial Pressure Ratio

There will be a pressure gradient along the pipes transmitting the wake and blade surface pressures to the rotor hub due to the centrifugal force on the mass of air in the pipes. The pressure difference between the Scanivalve transducers located on the rotor axis and the pressure holes on the blade must be calculated. Considering the equilibrium of an element of air in the tube at radius r

$$\delta p = \rho \Omega^2 r \, \delta r.$$

Writing ρ in terms of T and integrating from the rotor hub to the pressure measuring radius gives

$$\int_{p_{root}}^{p_r} \frac{dp}{p} = \Omega^2 \frac{\rho_0 T_0}{p_0} \int_0^r \frac{r}{T} dr.$$

In order to integrate this expression the temperature distribution must be specified. If the temperature is assumed constant along the pressure tube then,

$$\frac{p_r}{p_{root}} = \exp\left[\frac{\Omega^2 r^2 \rho_0 T_0}{2 p_0 T}\right].$$

For the hovering case it is convenient to write this expression in terms of the local stream Mach number (M), of the blade at radius r. If the pressure tube temperature is equal to the ambient air temperature and $\gamma = 1{\cdot}4$, then

$$\frac{p_r}{p_{root}} = \exp\left[0{\cdot}7 \, M^2\right].$$

Since the pressure tubes are buried just inside the nose of the blade their temperature may be raised by kinetic heating. For a temperature along the pressure tube equal to the local stagnation temperature at the blade leading edge integration of the expressions gives:

$$\frac{p_r}{p_{root}} = (1 + 0{\cdot}2 \, M^2)^{3{\cdot}5}.$$

In steady flight test conditions, when temperatures are steady throughout the blade structure, the actual temperature distribution must clearly lie between these two simplified distributions, but the exact temperature at different points in the blade is unknown. The above expressions may be expanded for comparison.

Tube temperature equal to outside air temperature. $\dfrac{p_r}{p_{root}} = 1 + 0{\cdot}7 \, M^2 + 0{\cdot}245 \, M^4 + \ldots.$

Tube temperature equal to leading edge stagnation temperature. $\dfrac{p_r}{p_{root}} = 1 + 0{\cdot}7 \, M^2 + 0{\cdot}175 \, M^4 + \ldots.$

This expansion shows that the calculated pressure ratio is not critically dependent on a precise knowledge of the temperature distribution in the blade. The isothermal calculation was used, as it was thought that it closely described the actual conditions, the possible error being less than 1 per cent. Values of p/H_0 on the blade are then calculated as follows:

$$\frac{p}{H_0} = 1 - \left[\frac{p_{root} \exp\left(0{\cdot}7 \, M^2\right)}{H_0}\right]$$

where

$$H_0 = p_0 + \tfrac{1}{2}\rho(\Omega r)^2(1 + 0{\cdot}25 \, M^2) \qquad \text{and} \qquad M = \frac{\Omega_r}{1117}\sqrt{\frac{288}{T_0}}.$$

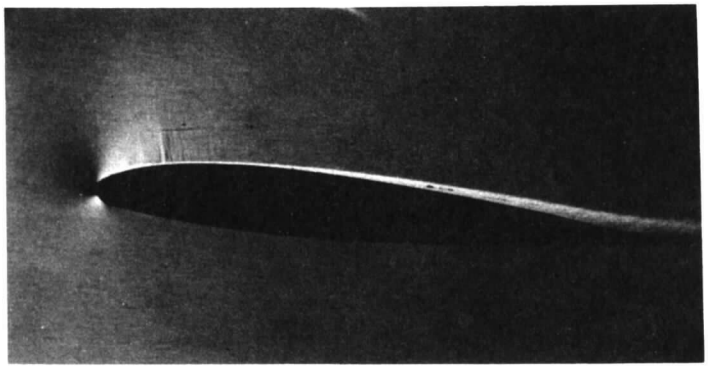

(a) RAE (NPL) 9615

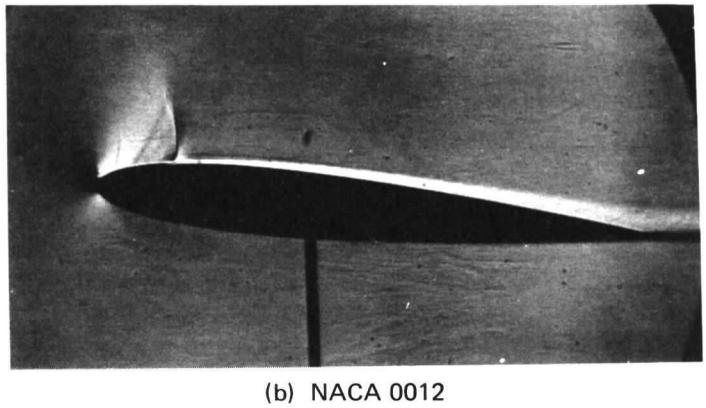

(b) NACA 0012

FIG. 1. Shock waves on two aerofoils at conditions typically encountered near blade tips in hover ($M = 0{\cdot}6$, $\alpha = 5{\cdot}8$ deg).

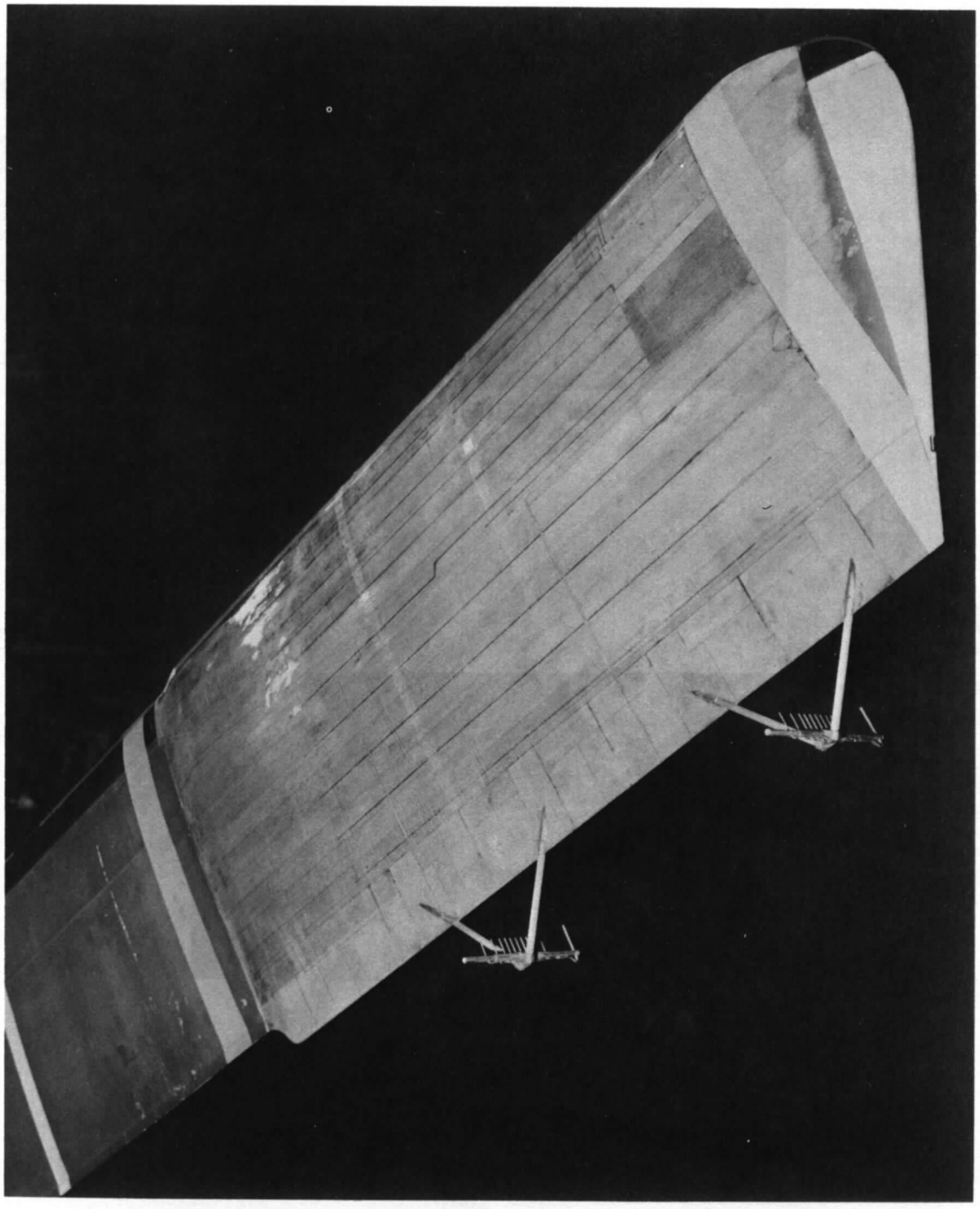

FIG. 2. Rotor blade glove with surface pressure tubes and wake pitot rakes.

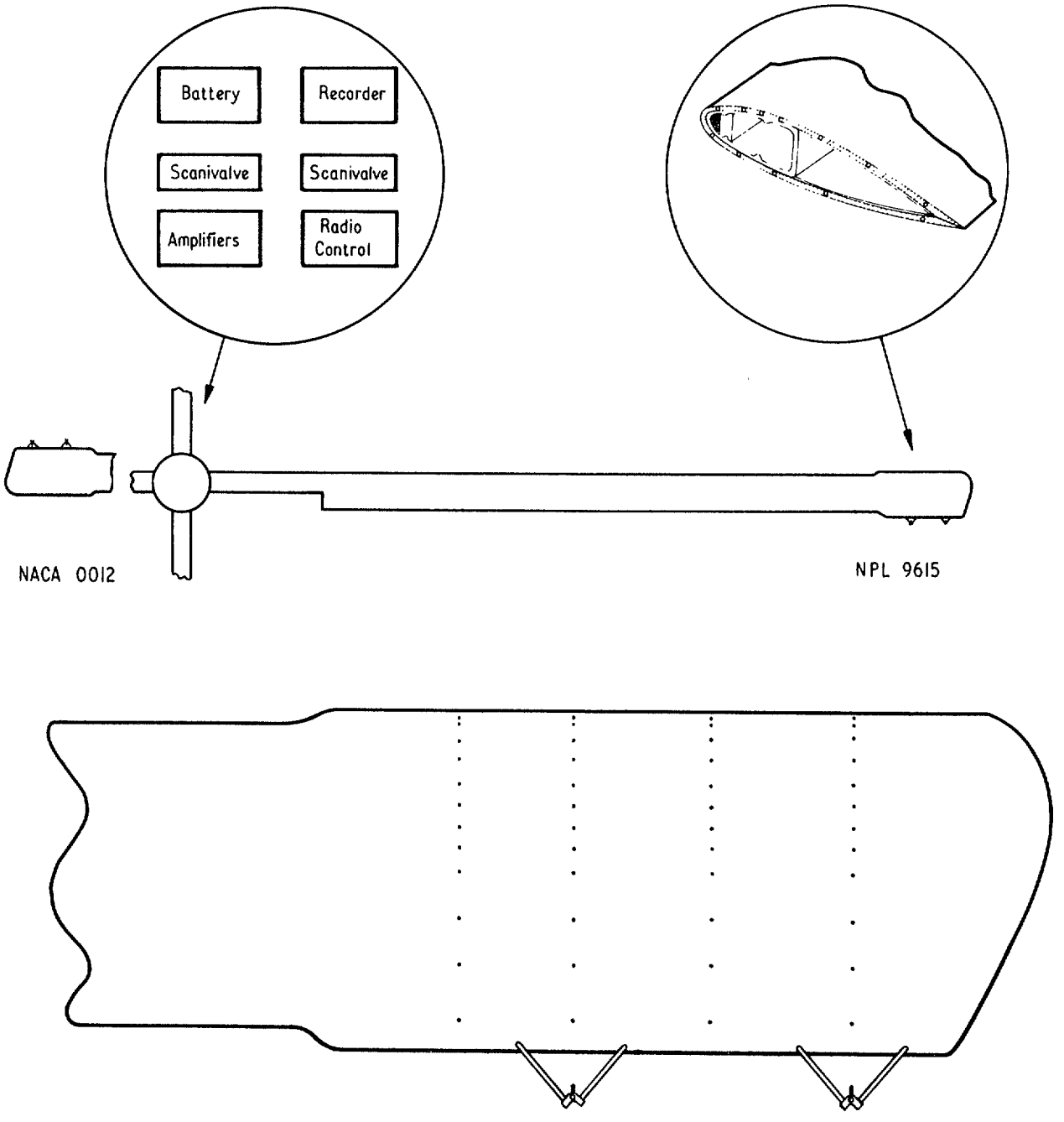

FIG. 3. Sketch of the blade modifications to the Wessex helicopter and of the hub-mounted recorder.

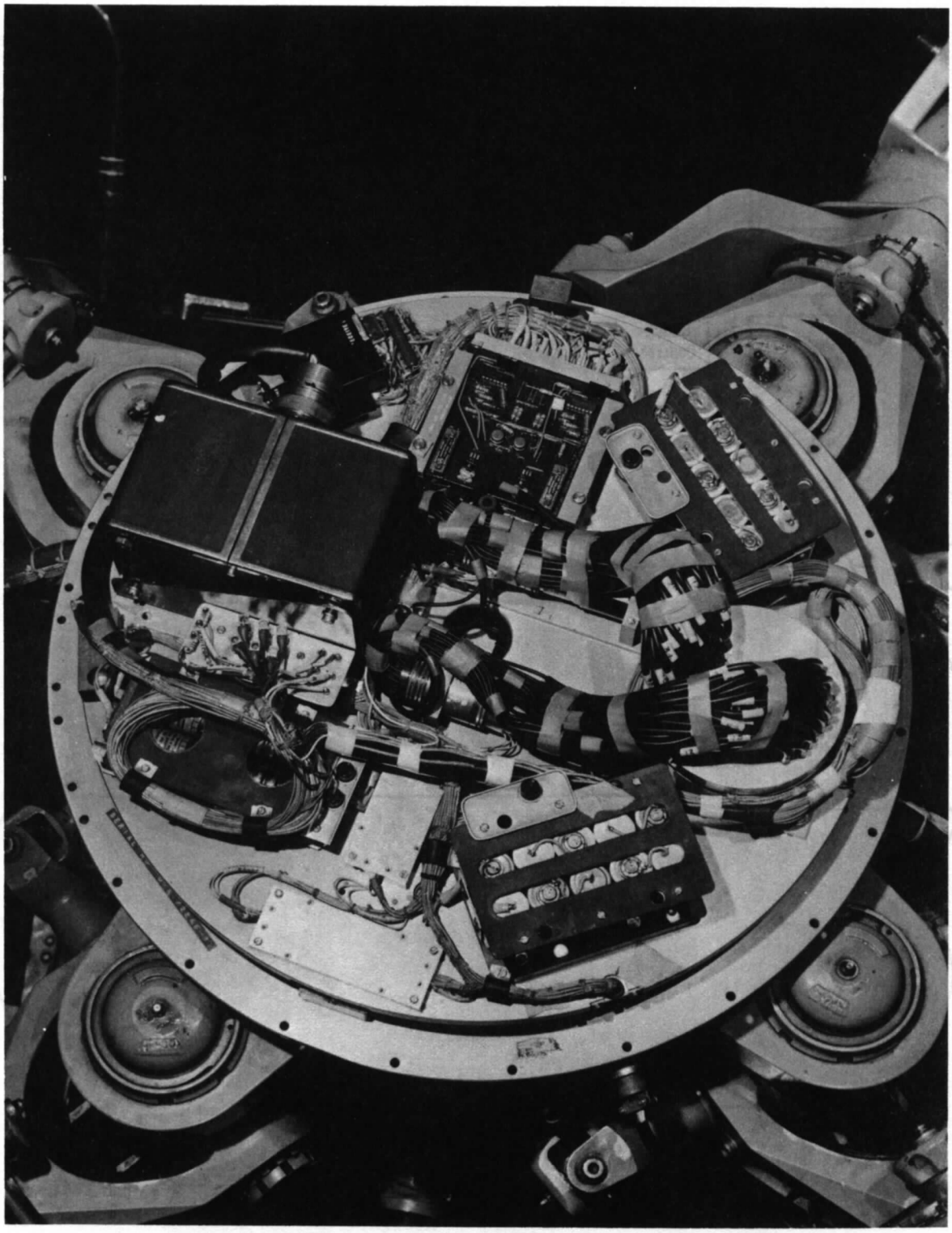

FIG. 4. Recorder assembly on rotor hub.

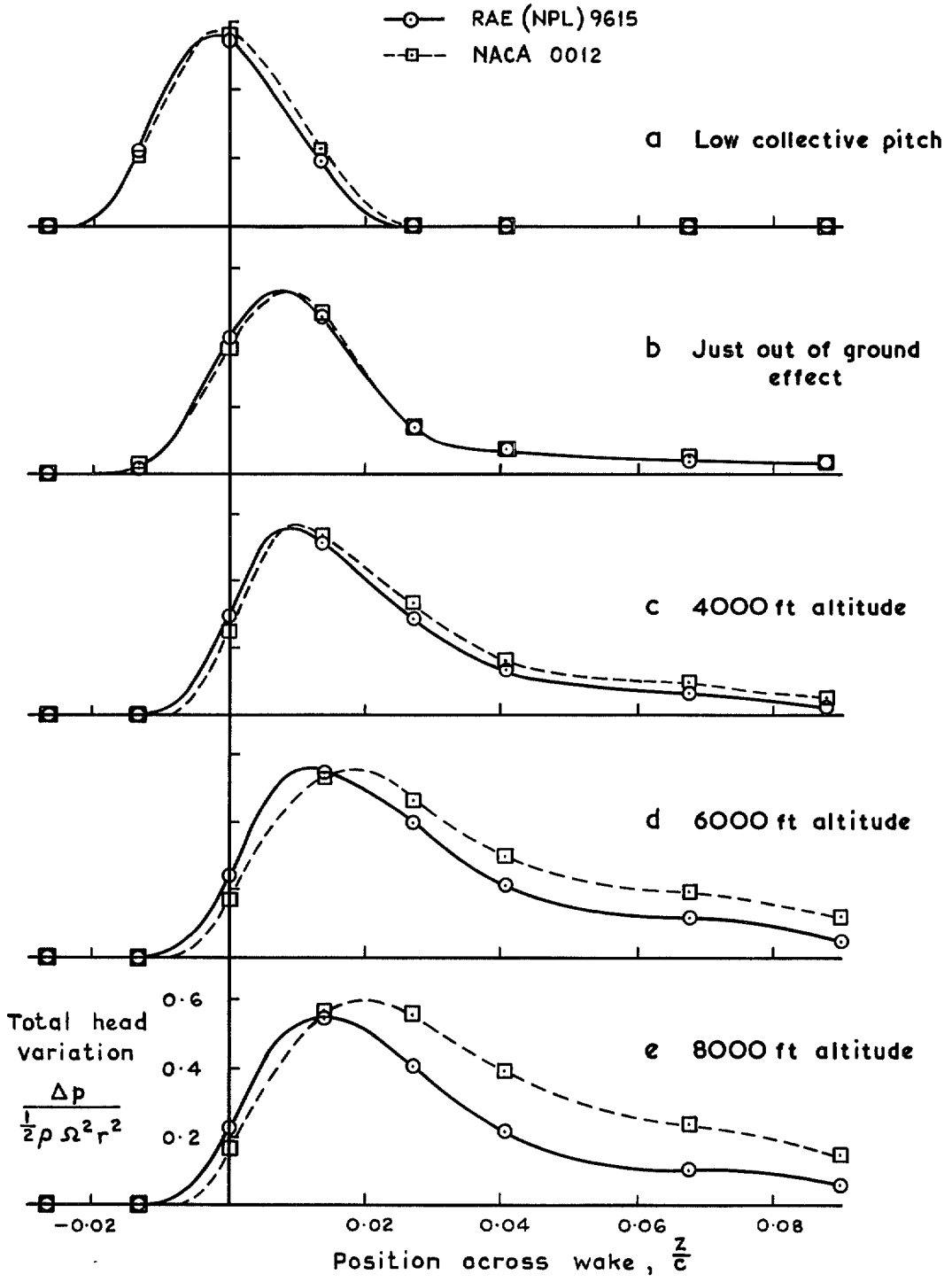

FIG. 5a–e. Measured wakes at $r/R = 0{\cdot}918$, for a range of rotor thrust coefficients.

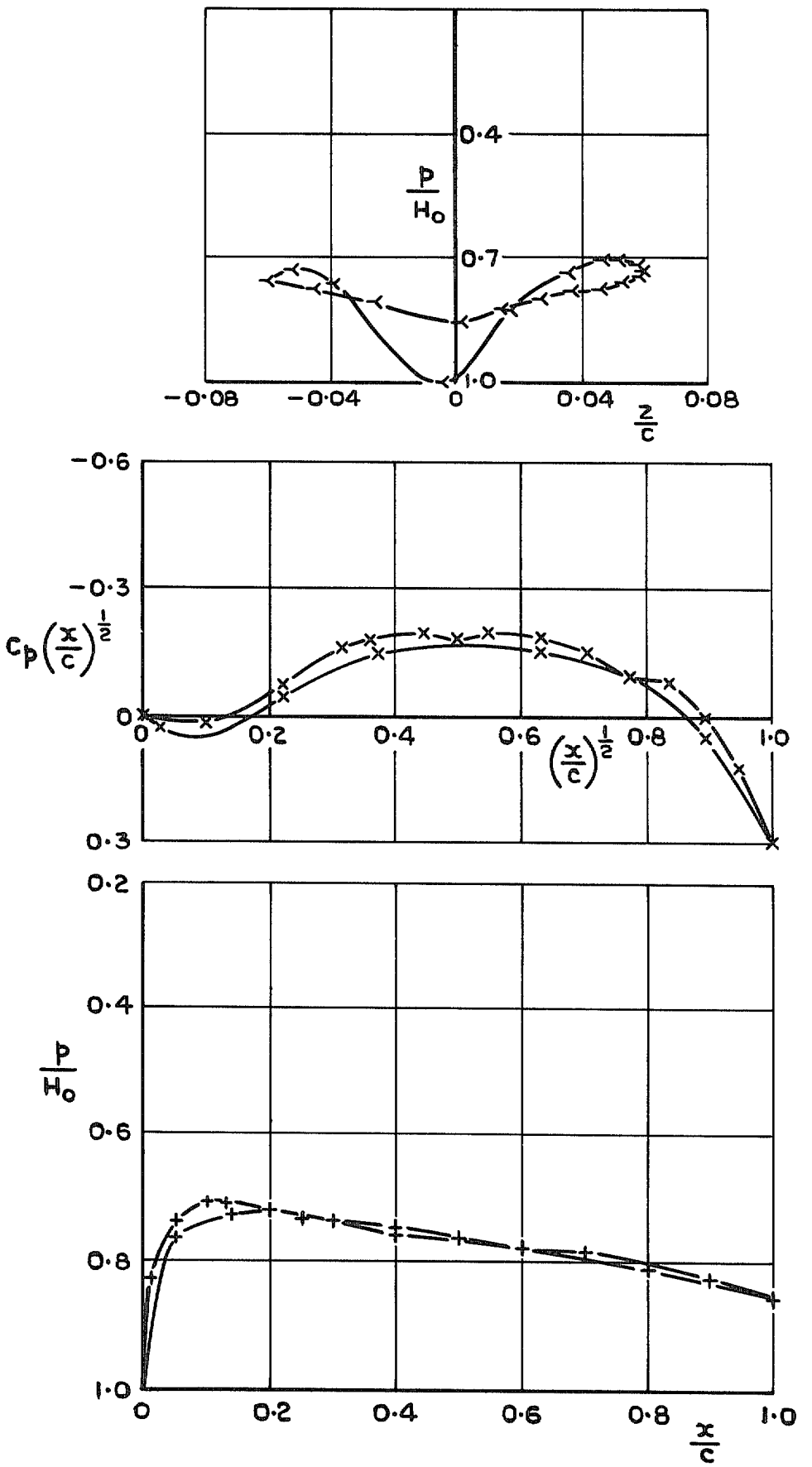

FIG. 6a. NACA 0012 surface pressure distributions minimum collective pitch. $\bar{C}_L = 0{\cdot}06, M = 0{\cdot}573$.

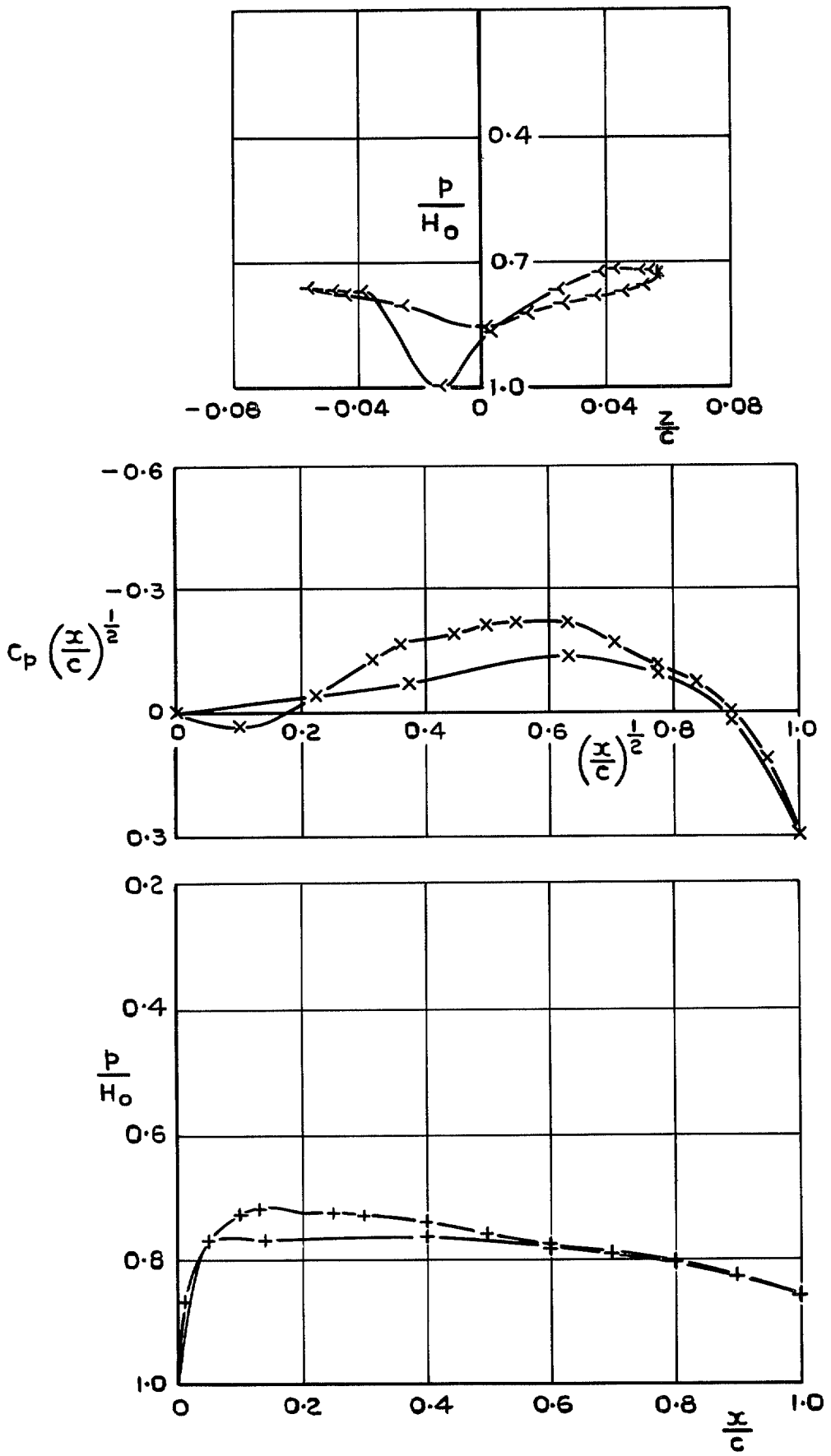

FIG. 6b. RAE(NPL)9615 surface pressure distributions minimum collective pitch. $\bar{C}_L = 0{\cdot}08$, $M = 0{\cdot}573$.

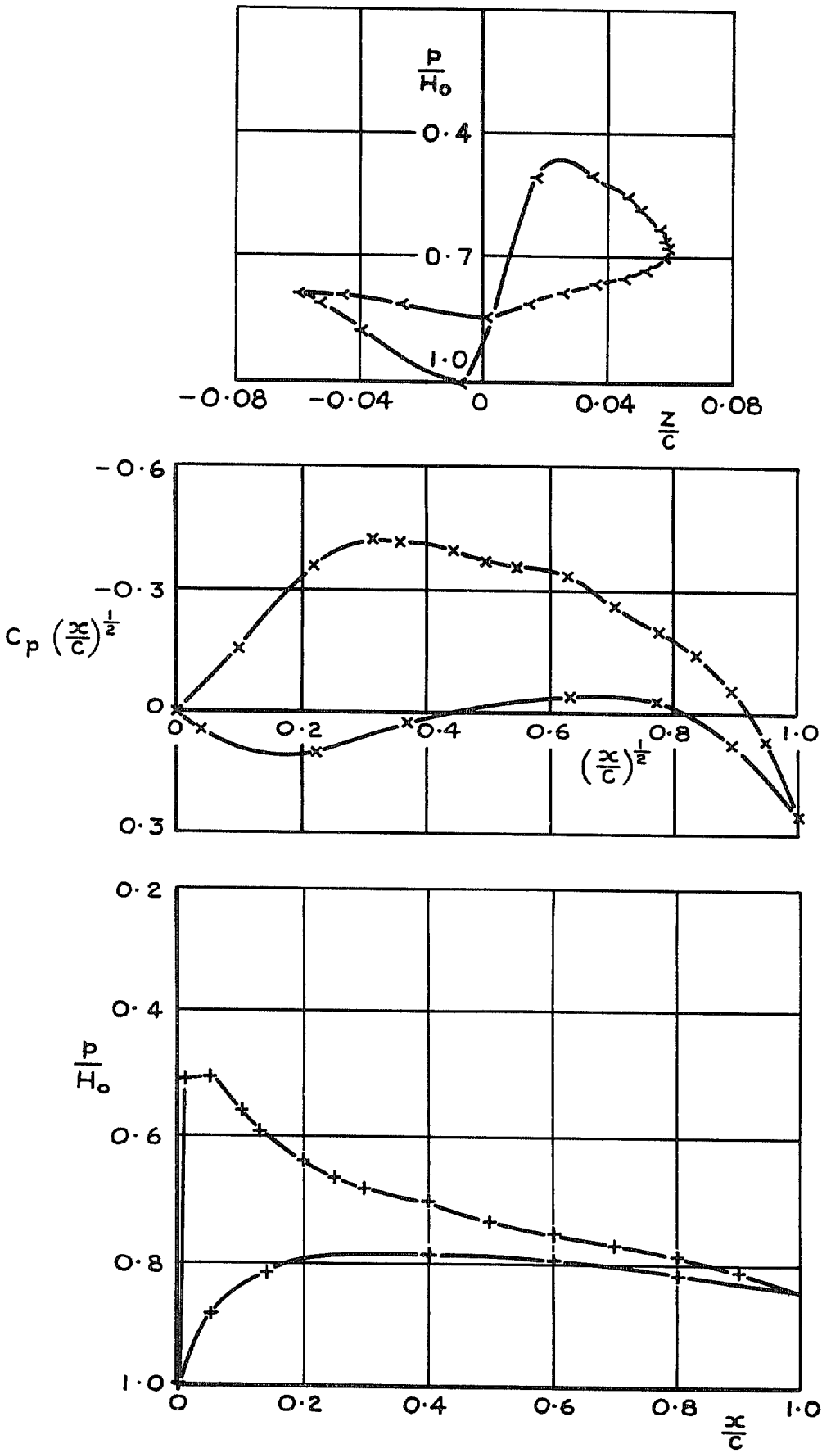

FIG. 7a. NACA 0012 surface pressure distributions. Just out of ground effect. $\bar{C}_L = 0{\cdot}56, M = 0{\cdot}573$.

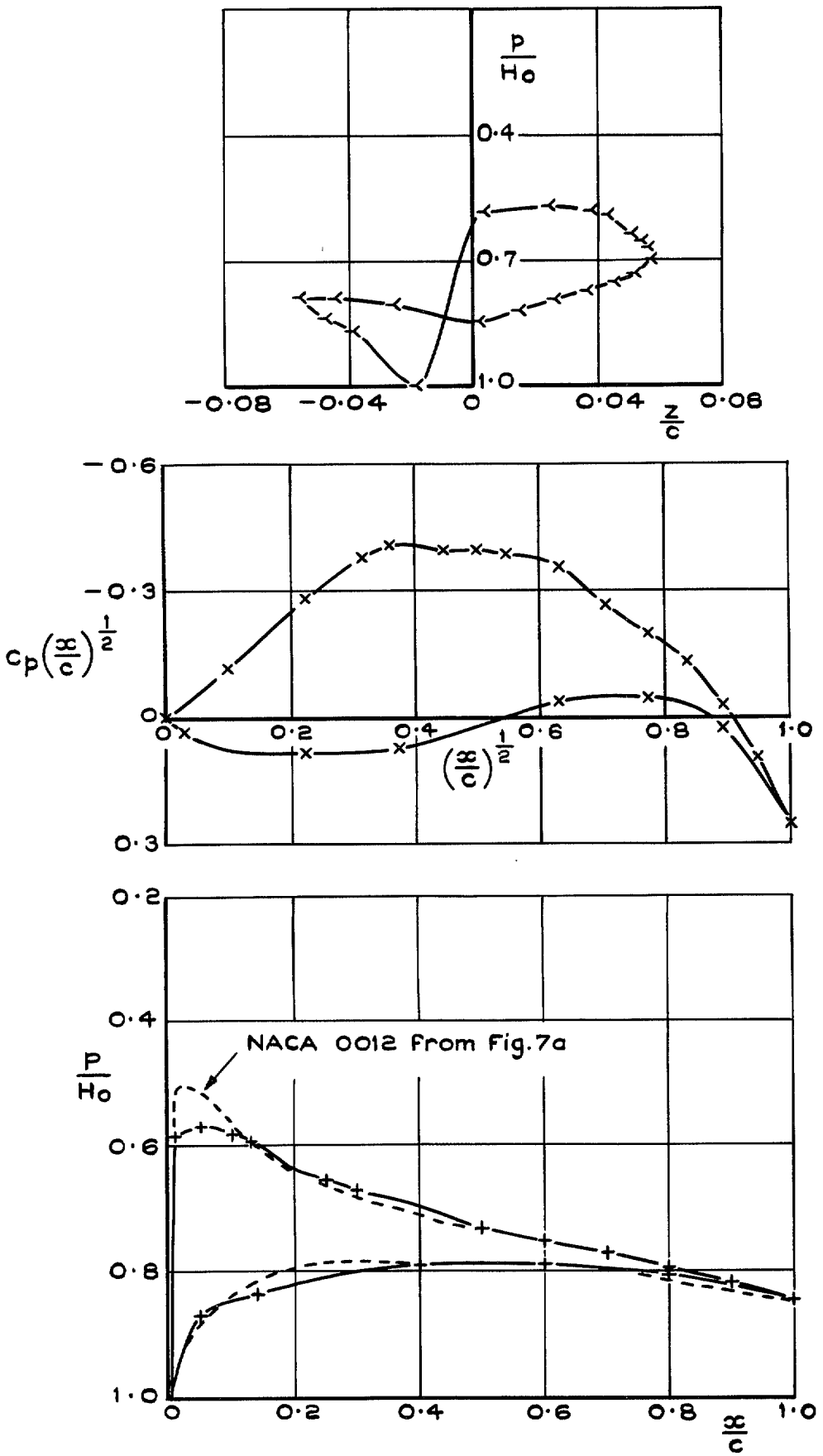

FIG. 7b. RAE(NPL) 9615 surface pressure distributions. Just out of ground effect. $\bar{C}_L = 0{\cdot}53$, $M = 0{\cdot}573$.

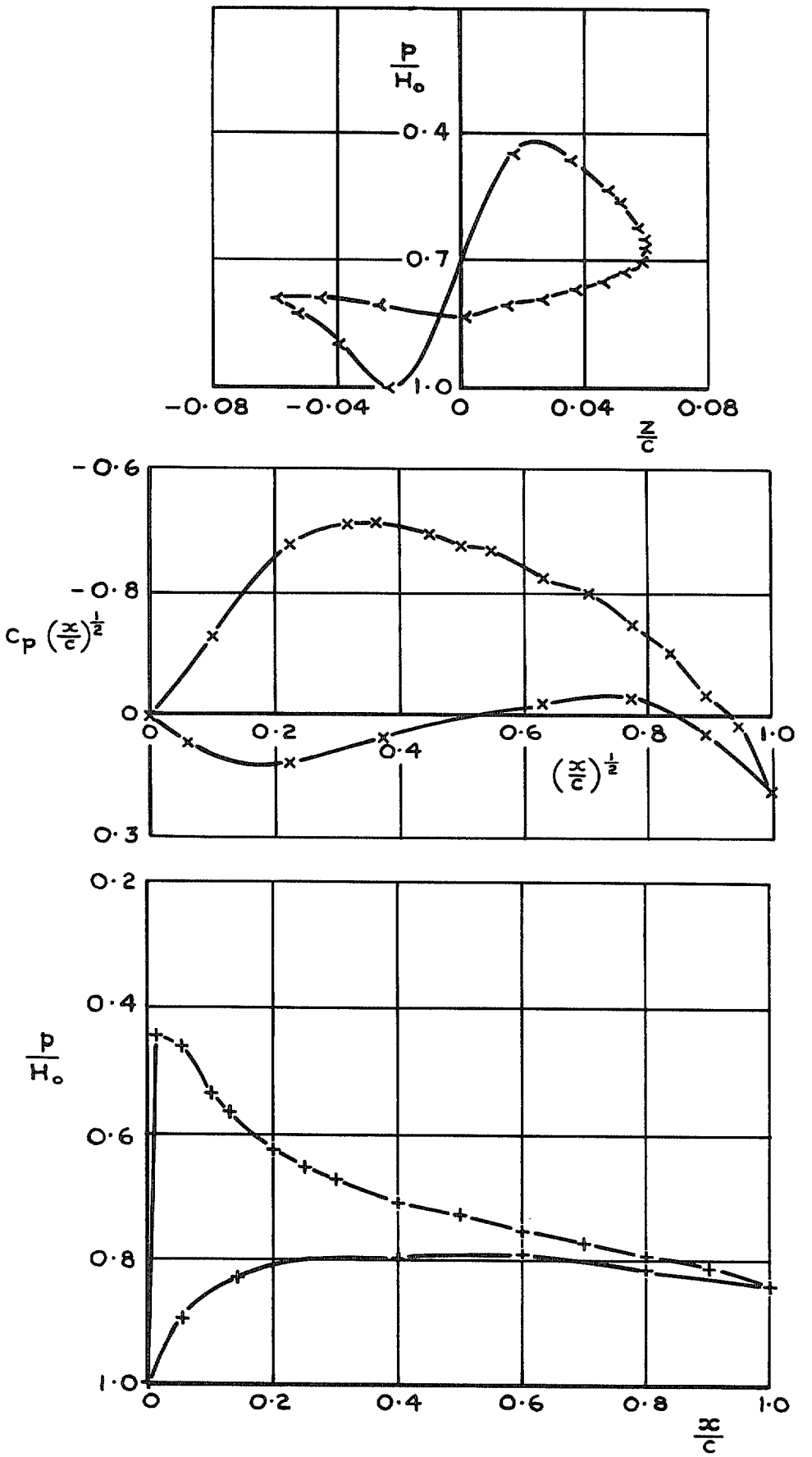

FIG. 8a. NACA 0012 surface pressure distributions at 8000 ft roughened L.E. $\bar{C}_L = 0{\cdot}63$, $M = 0{\cdot}570$.

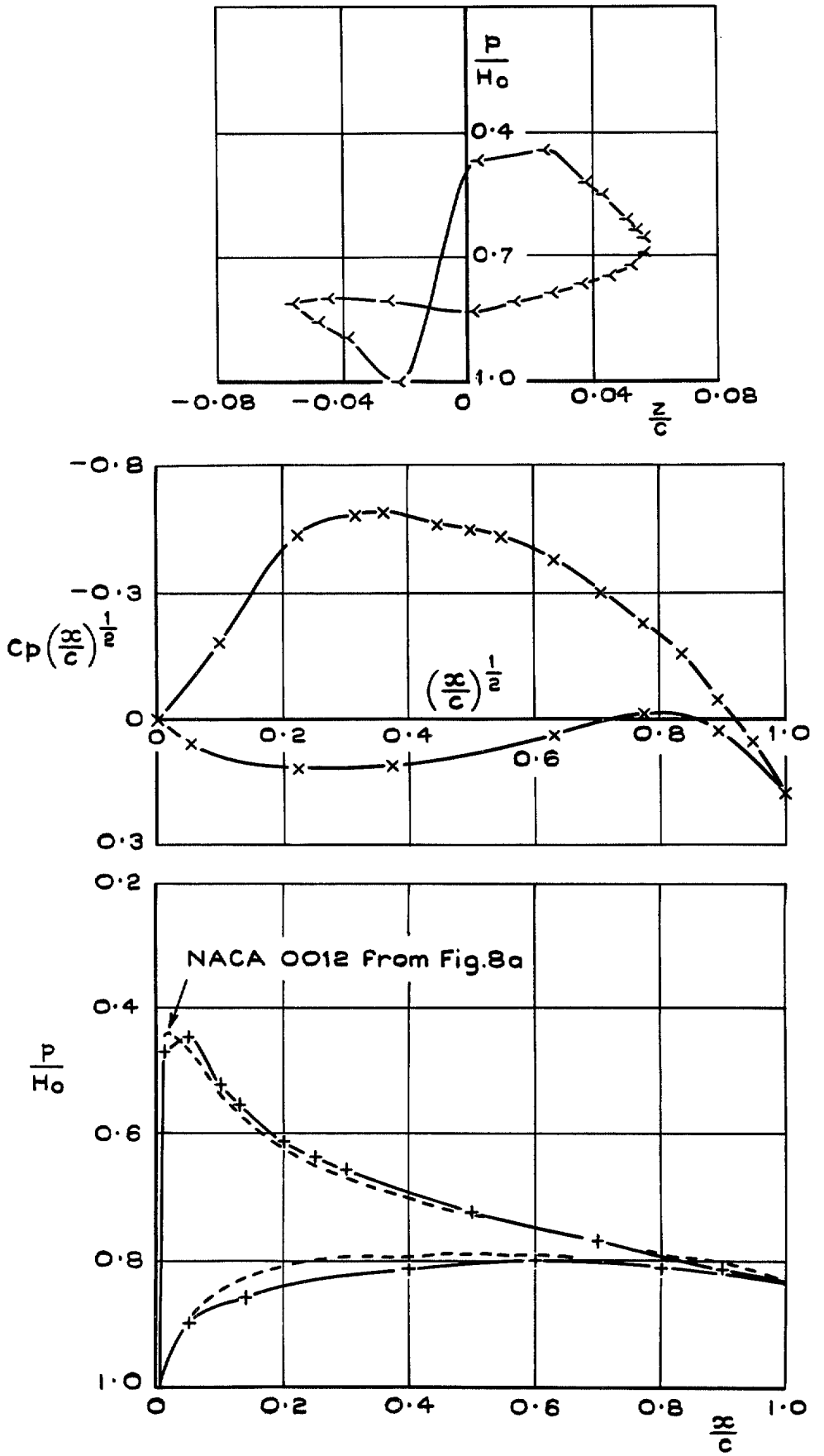

FIG. 8b. RAE(NPL)9615 surface pressure distributions at 8000 ft roughened L.E. $\bar{C}_L = 0{\cdot}71, M = 0{\cdot}570$.

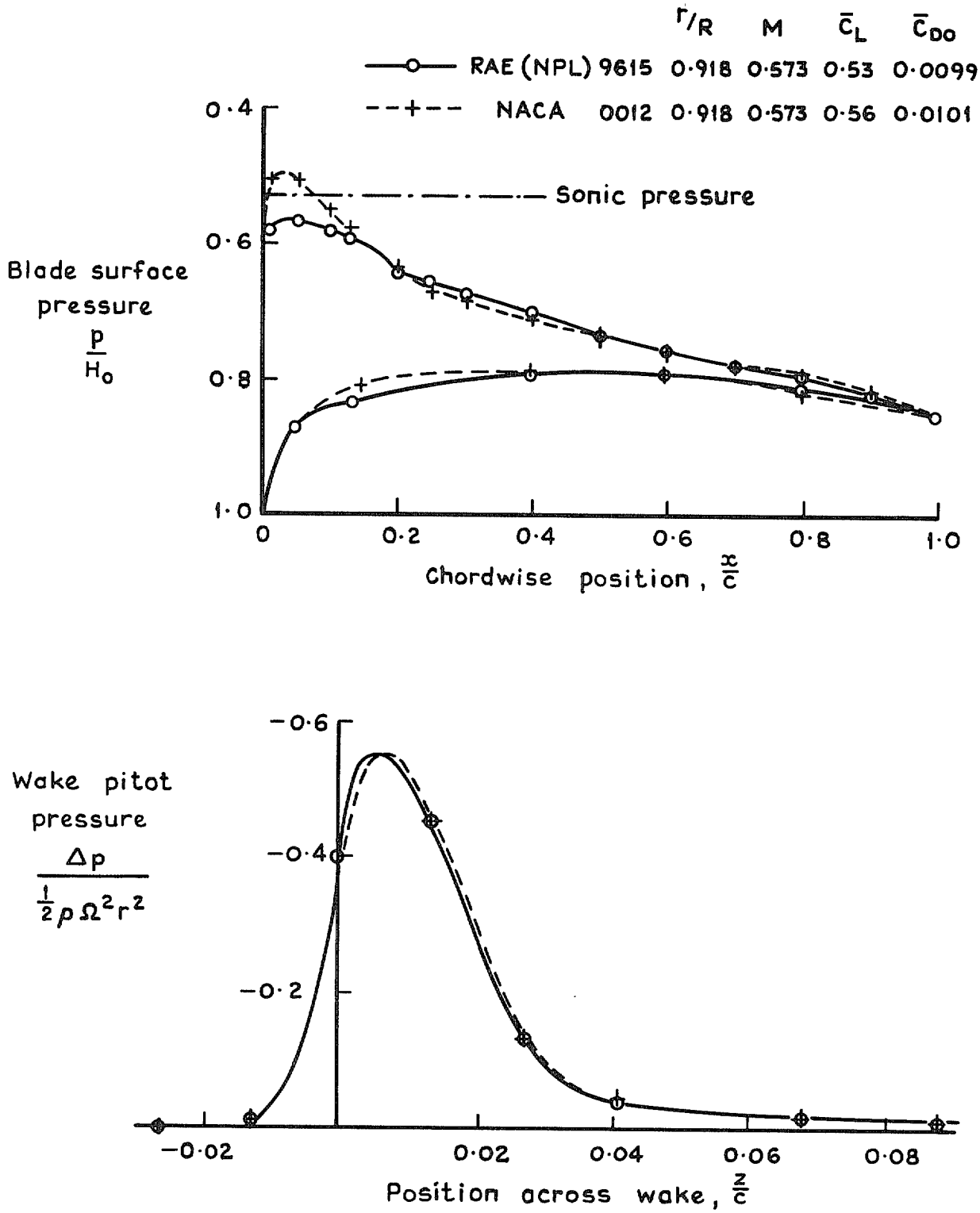

FIG. 9. Comparison of mean surface and wake pressures measured simultaneously in hovering flight: below drag divergence.

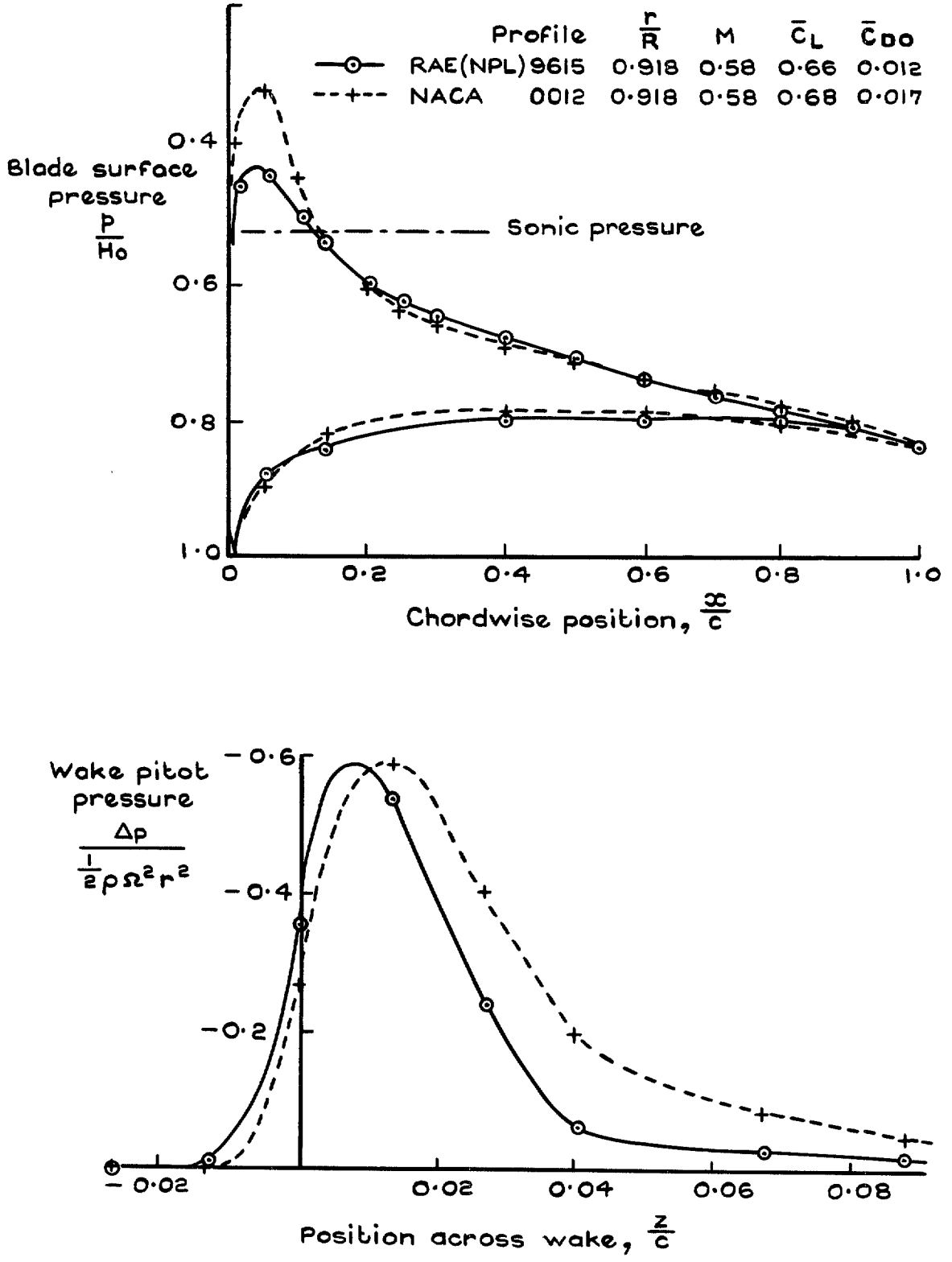

FIG. 10. Comparison of mean surface and wake pressures measured simultaneously in hovering flight: above drag divergence.

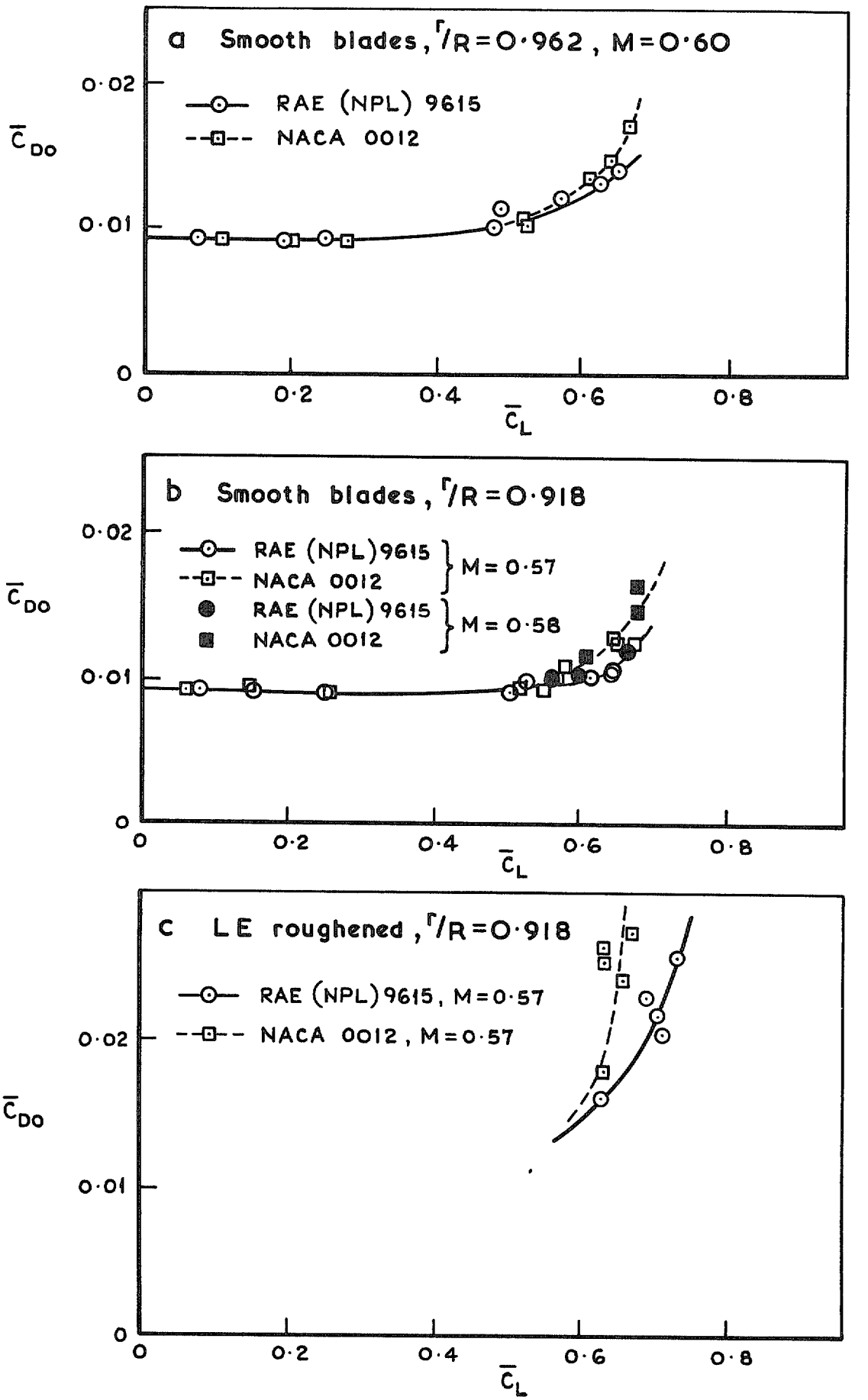

FIG. 11a–c. Measured lift-drag polars for the two test sections.

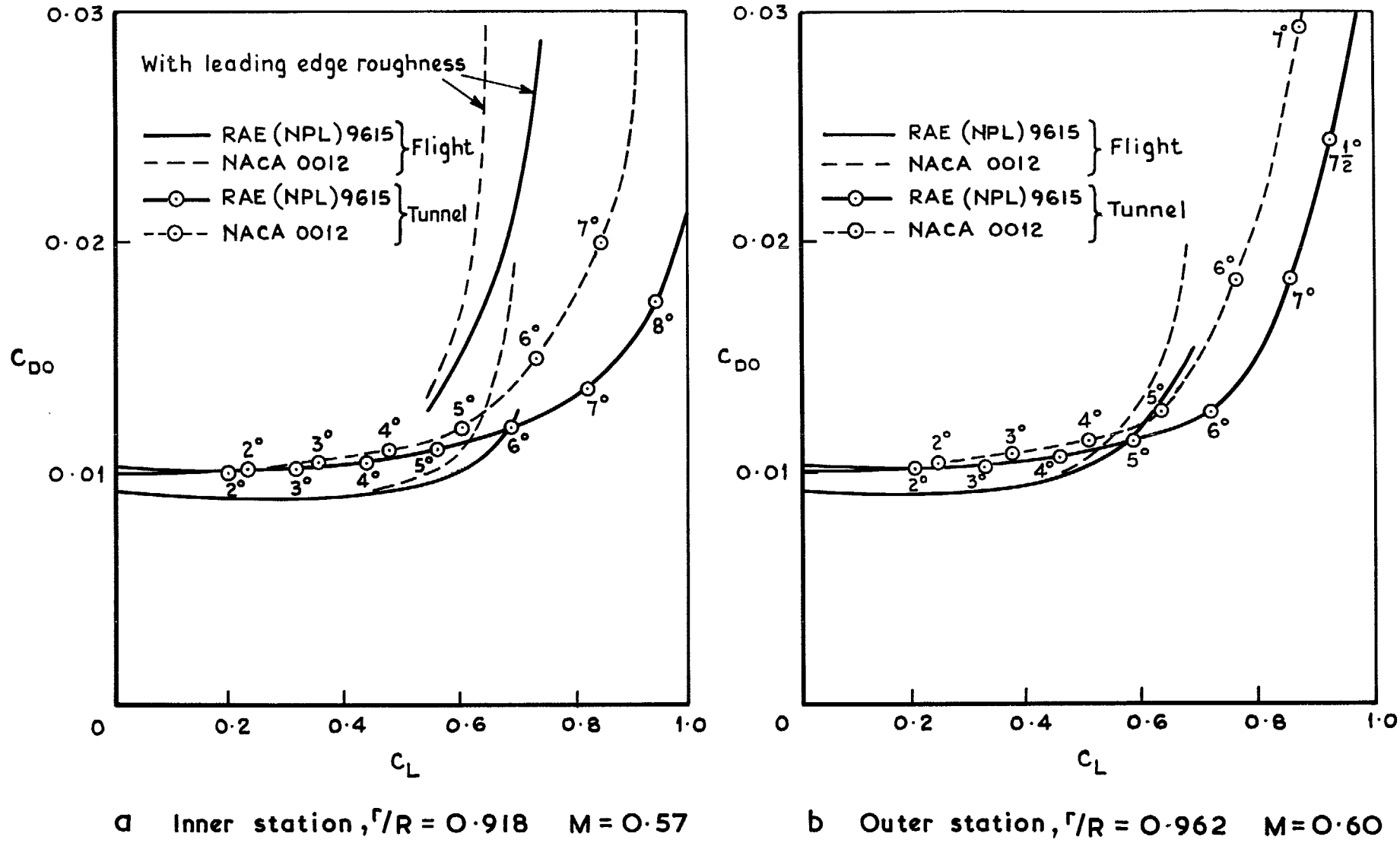

FIG. 12a, b. Flight measurements compared with wind tunnel drag 'polars'.

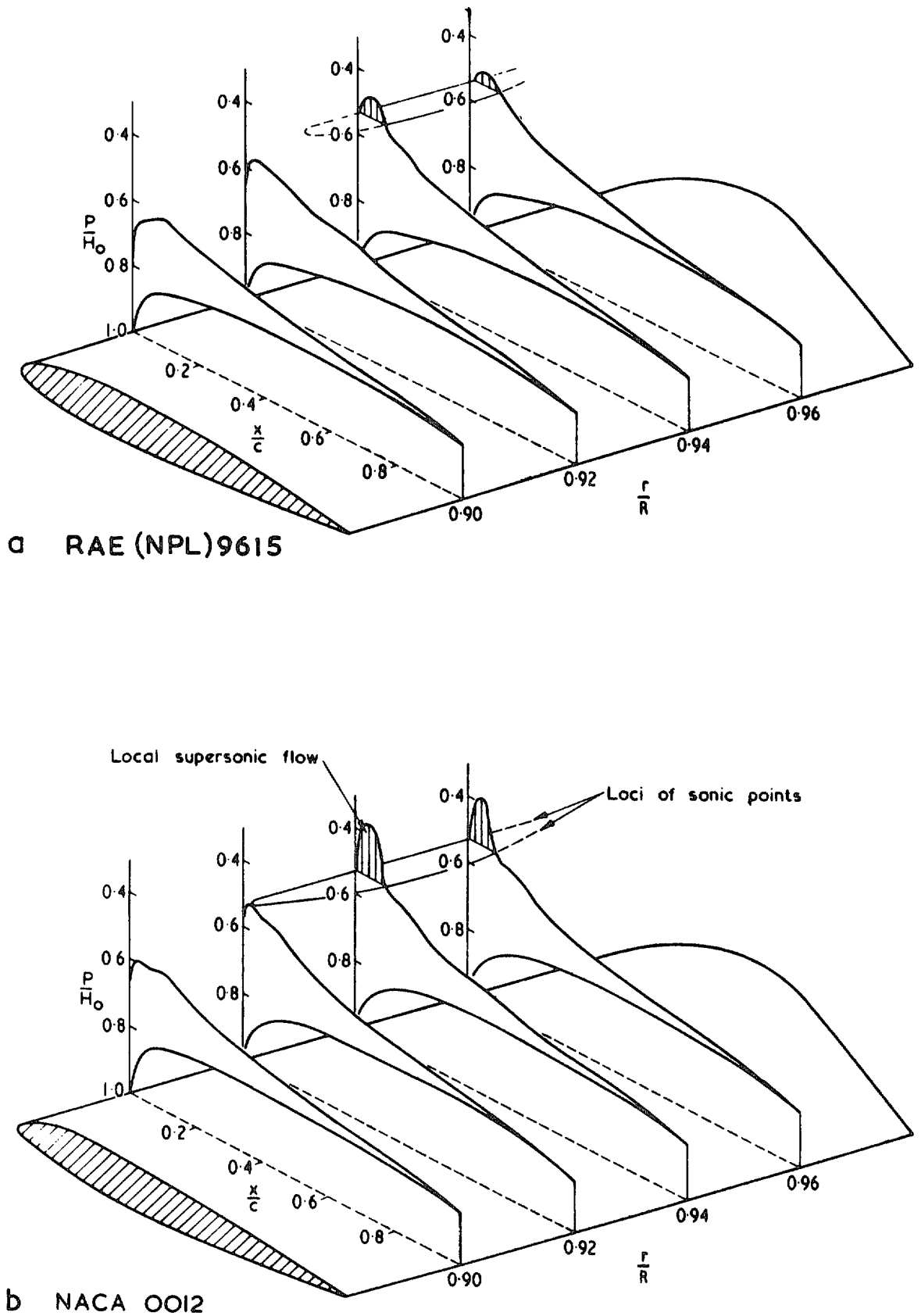

FIG. 13a, b. Pressure distributions on outer portions of two blades with different sections (low altitude hover).

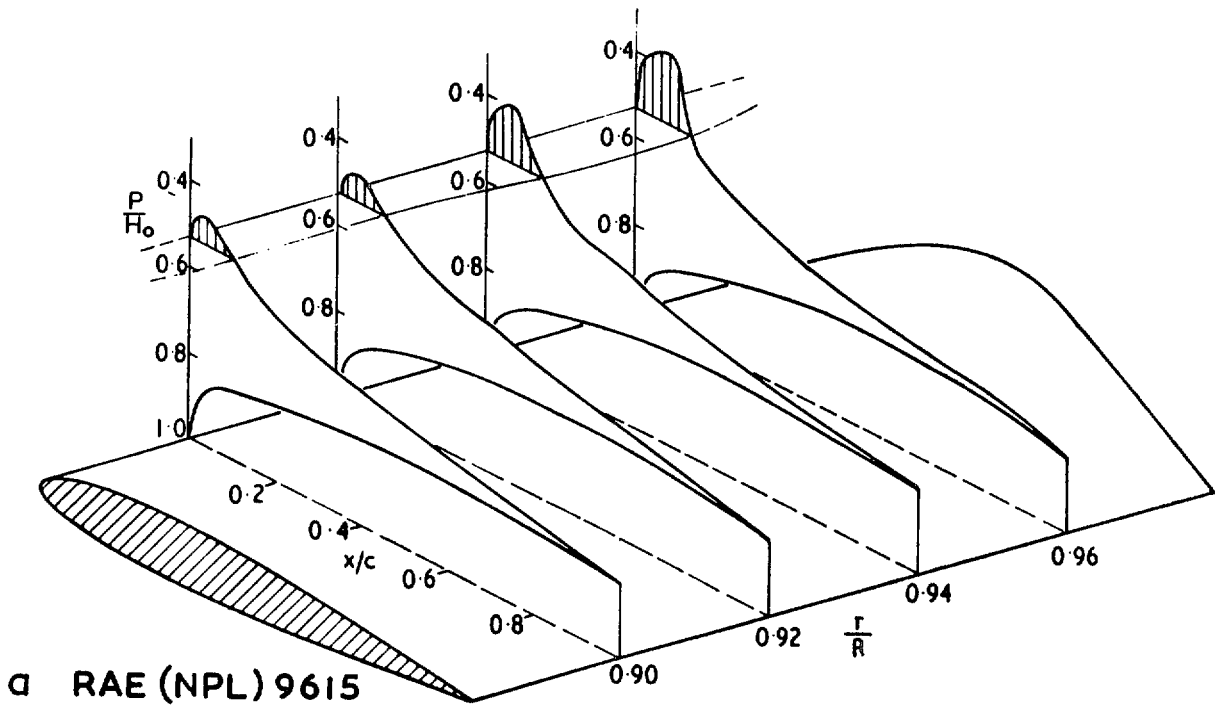

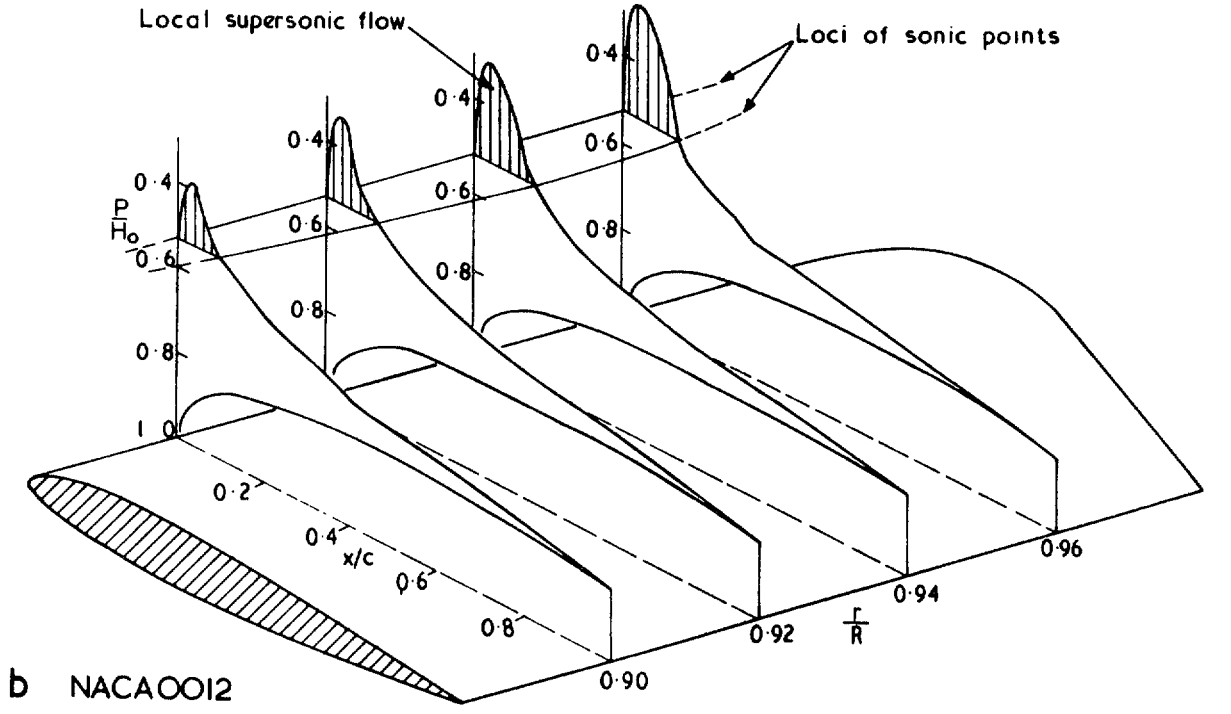

FIG. 14a, b. Pressure distributions on outer portion of two blades with different sections (high altitude hover).

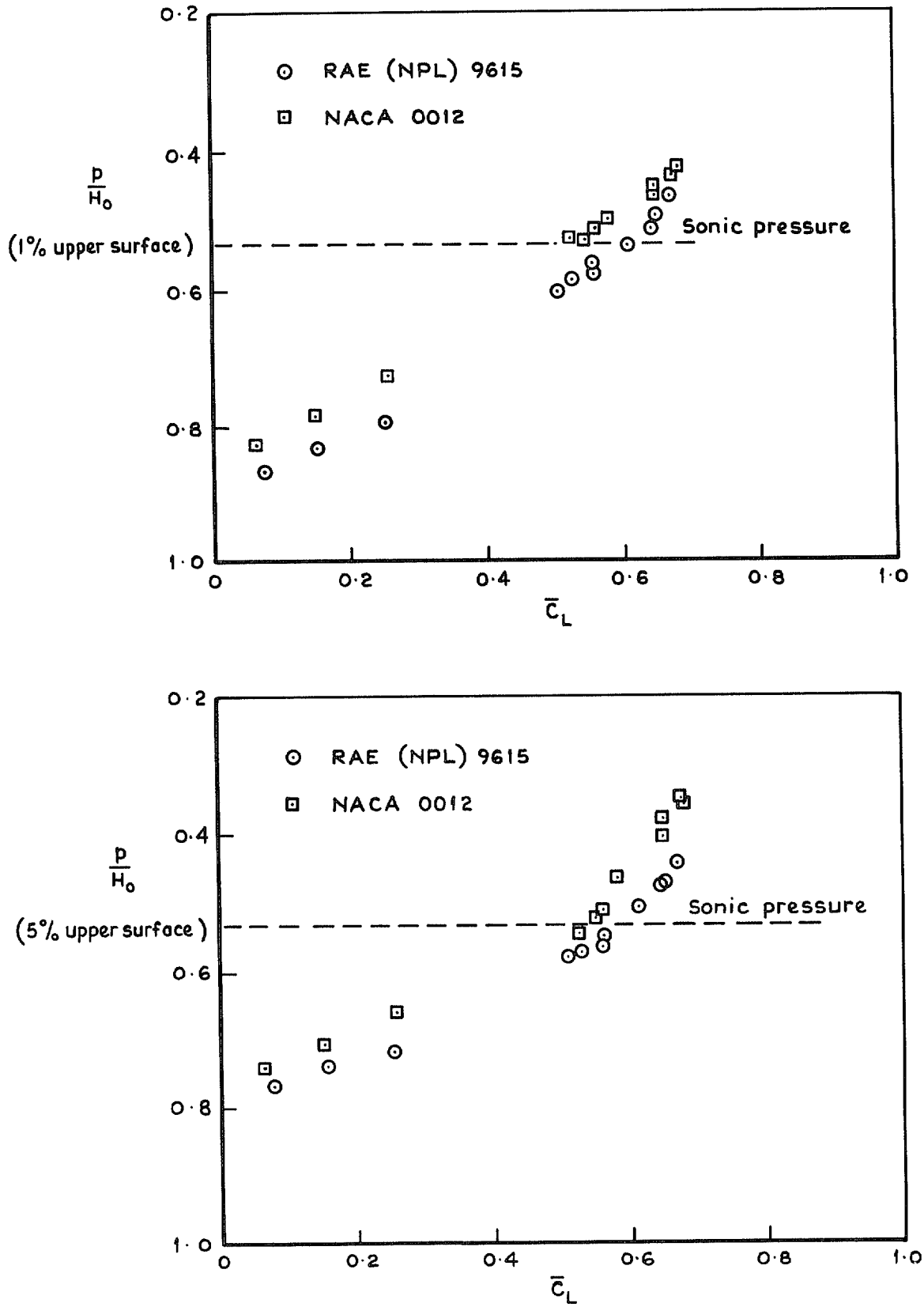

FIG. 15. Flight measurements illustrating the difference in suction peak height on the two profiles, at $r/R = 0{\cdot}918$.

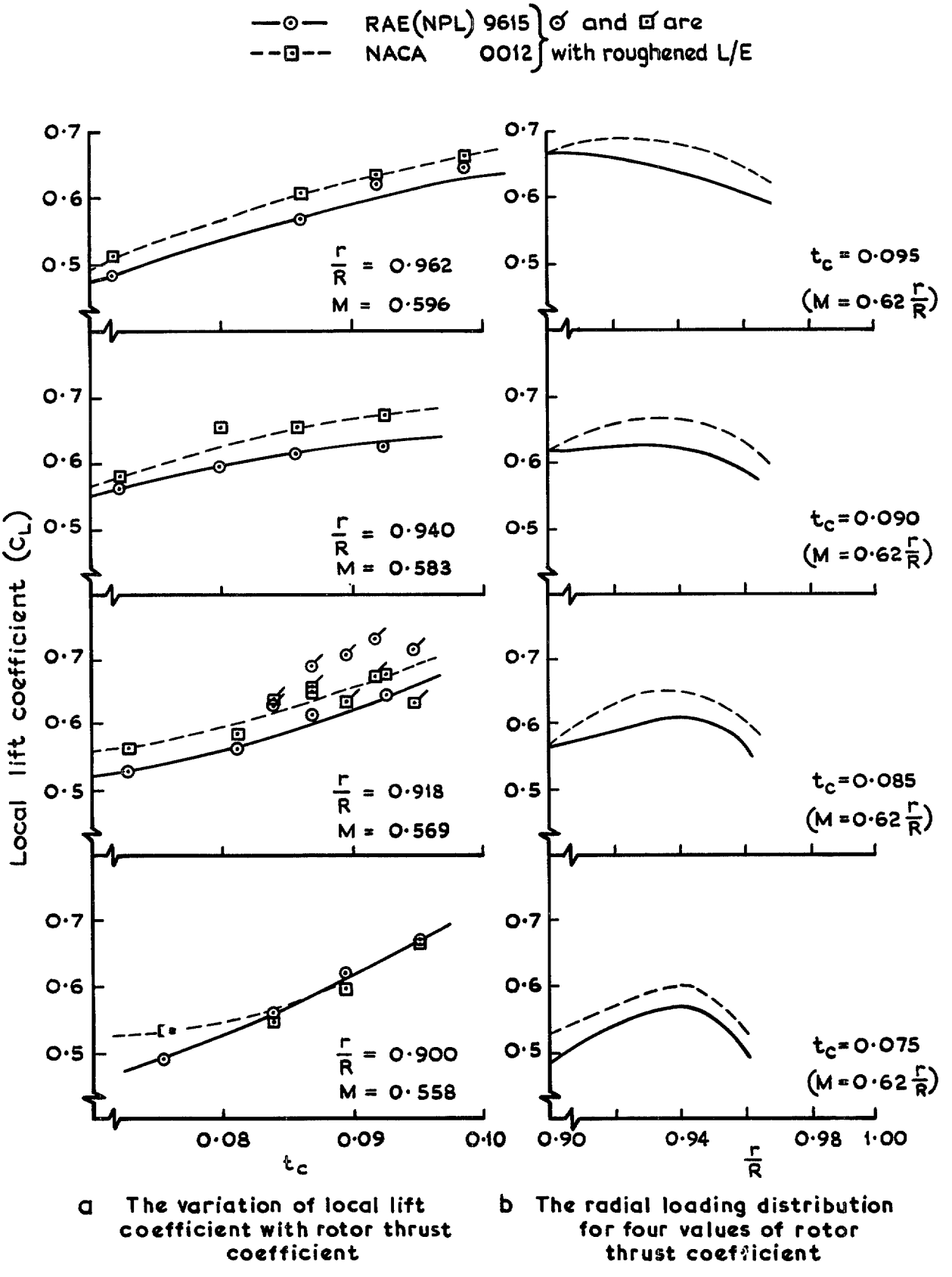

a The variation of local lift coefficient with rotor thrust coefficient

b The radial loading distribution for four values of rotor thrust coefficient

FIG. 16a, b. Lift coefficients derived from integrated mean pressures.

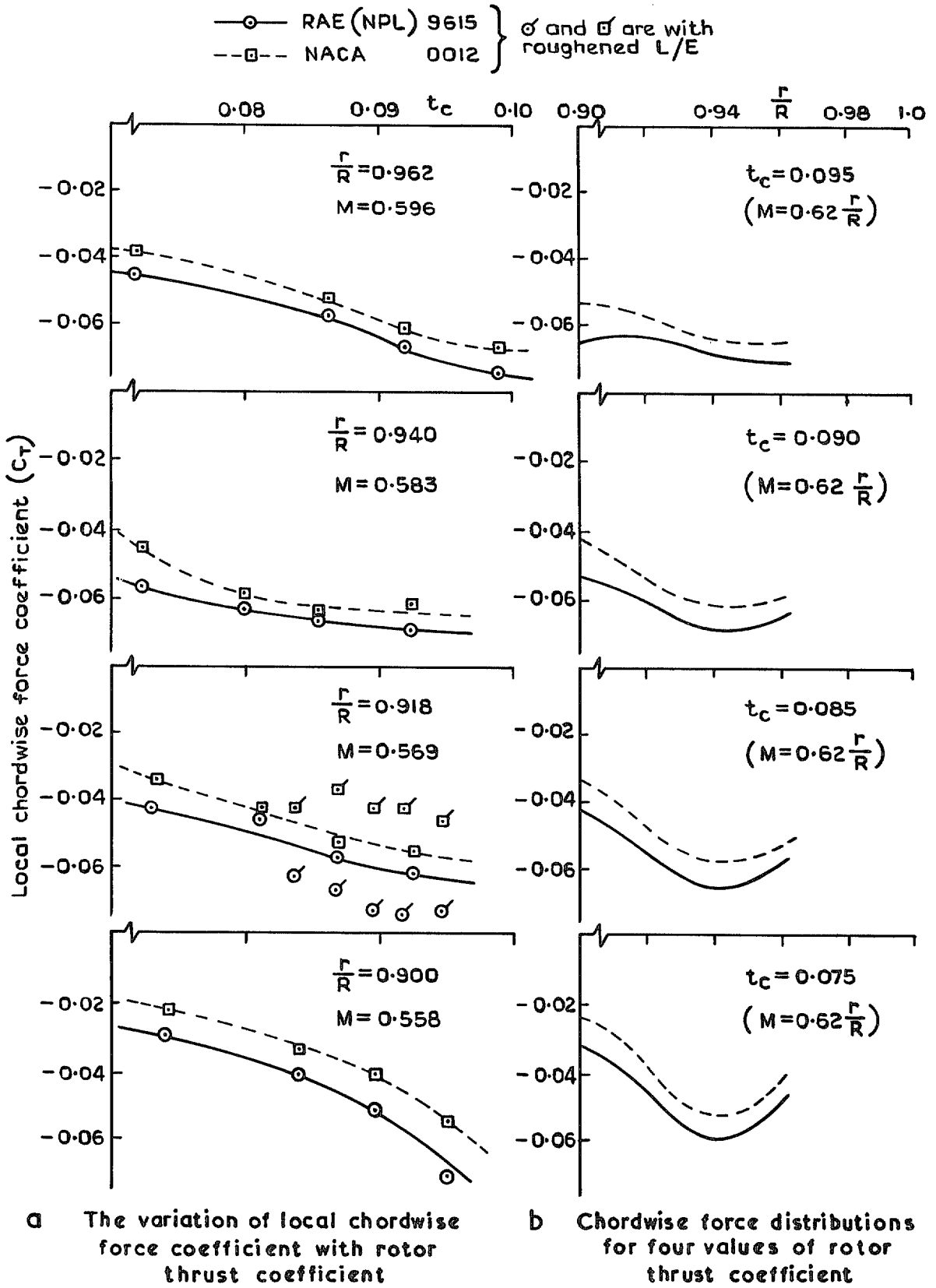

a The variation of local chordwise force coefficient with rotor thrust coefficient

b Chordwise force distributions for four values of rotor thrust coefficient

FIG. 17a, b. Integrated mean pressures resolved chordwise (C_T).

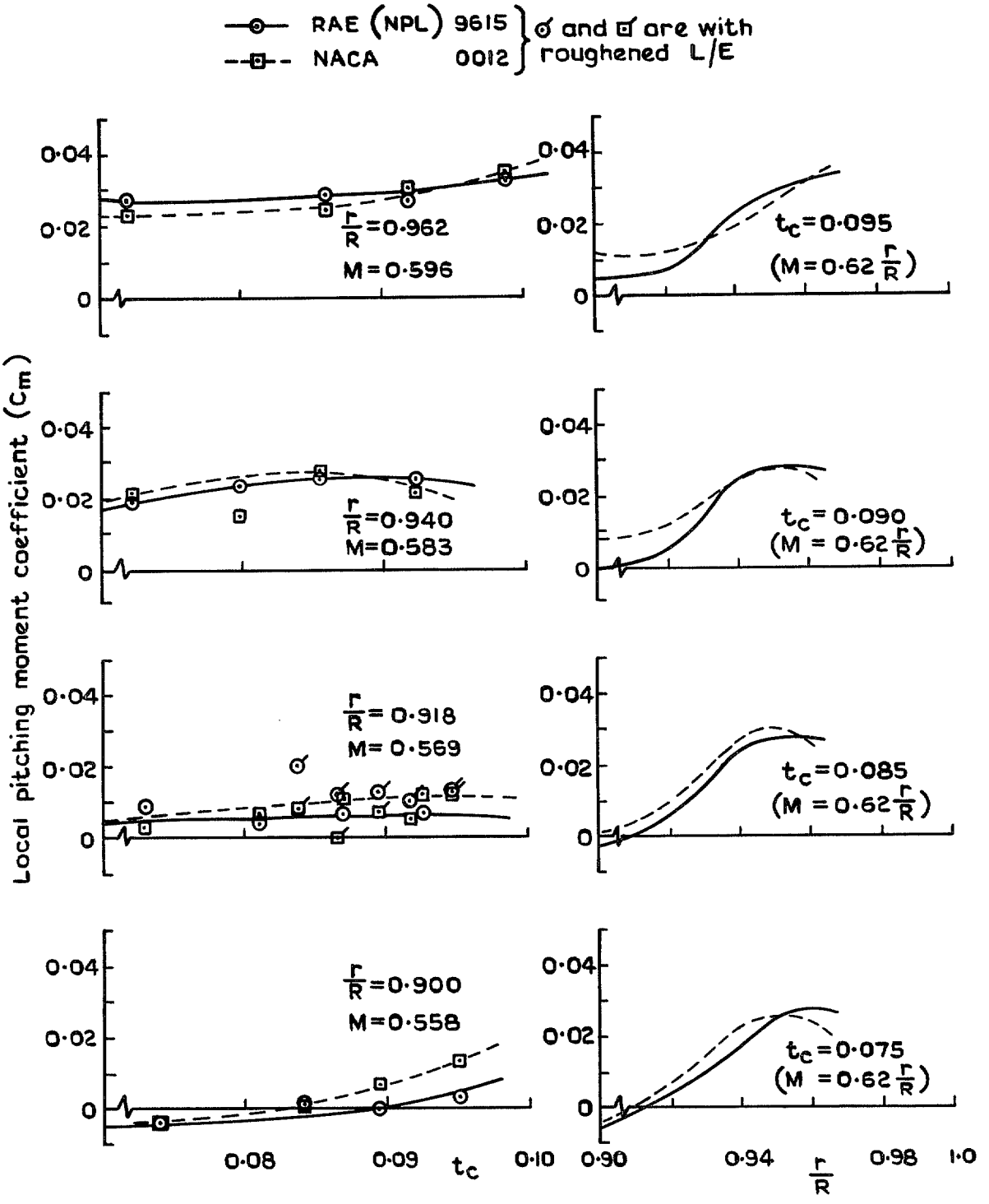

a The variation of local pitching moment coefficient with rotor thrust coefficient

b Pitching moment distributions for four values of rotor thrust coefficient

FIG. 18a, b. Pitching moments derived from integrated pressures.

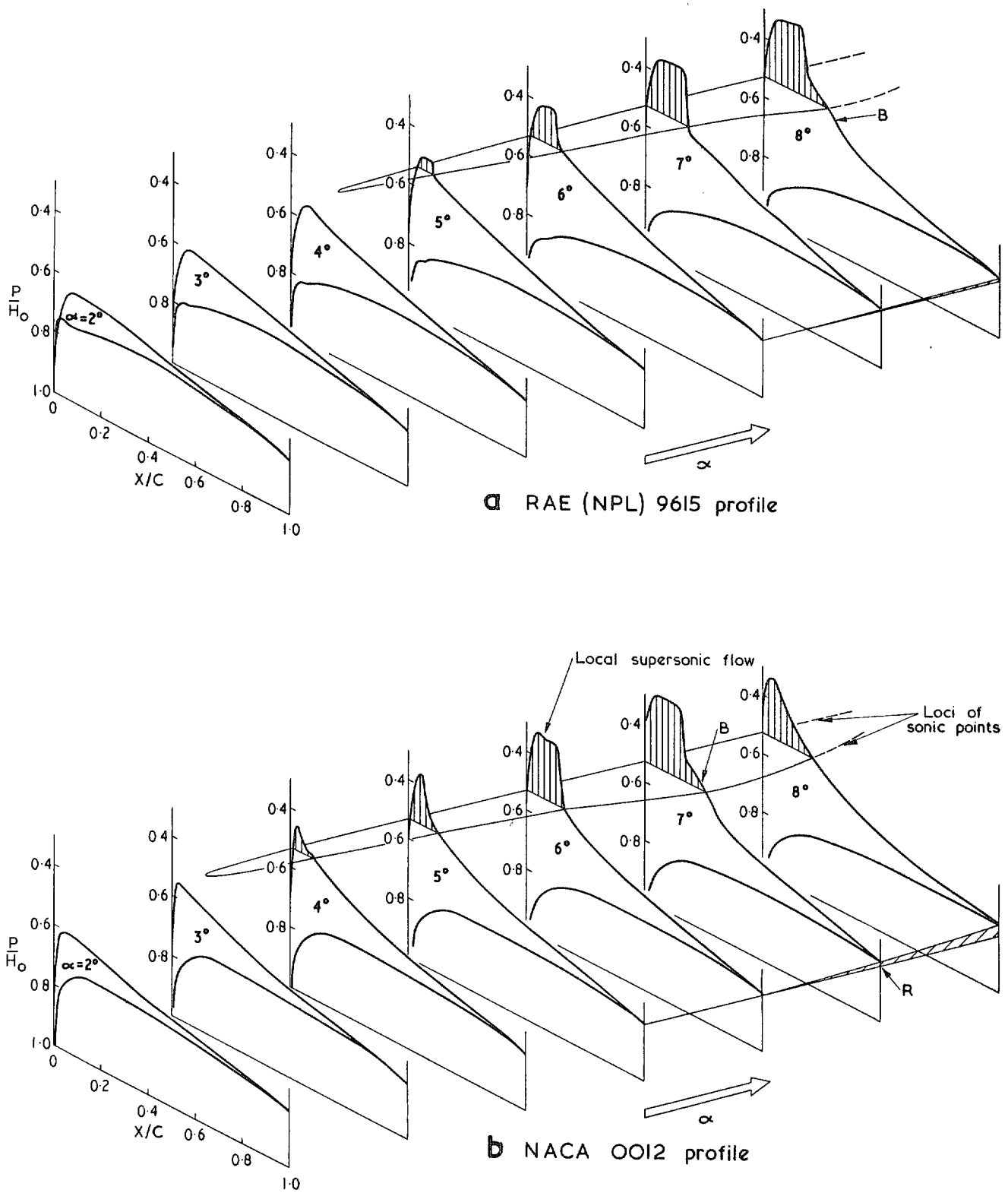

FIG. 19a, b. Two-dimensional wind-tunnel measurements showing the development of surface pressure distributions with increasing incidence at $M_0 = 0{\cdot}6$. (Typical tip Mach number for hover.)

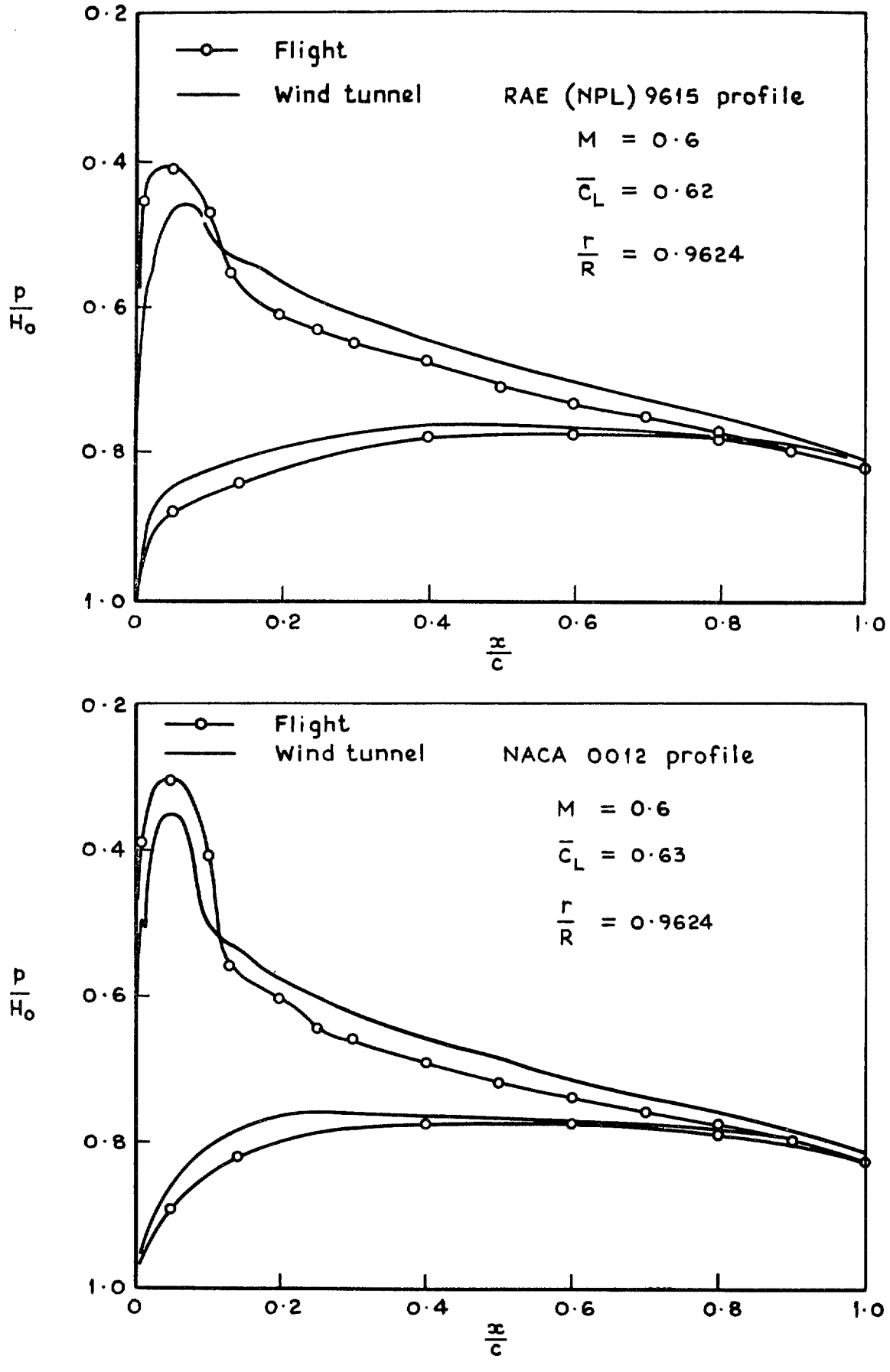

FIG. 20. Comparison of surface pressure distributions with wind tunnel measurements at the same lift coefficient and Mach number.

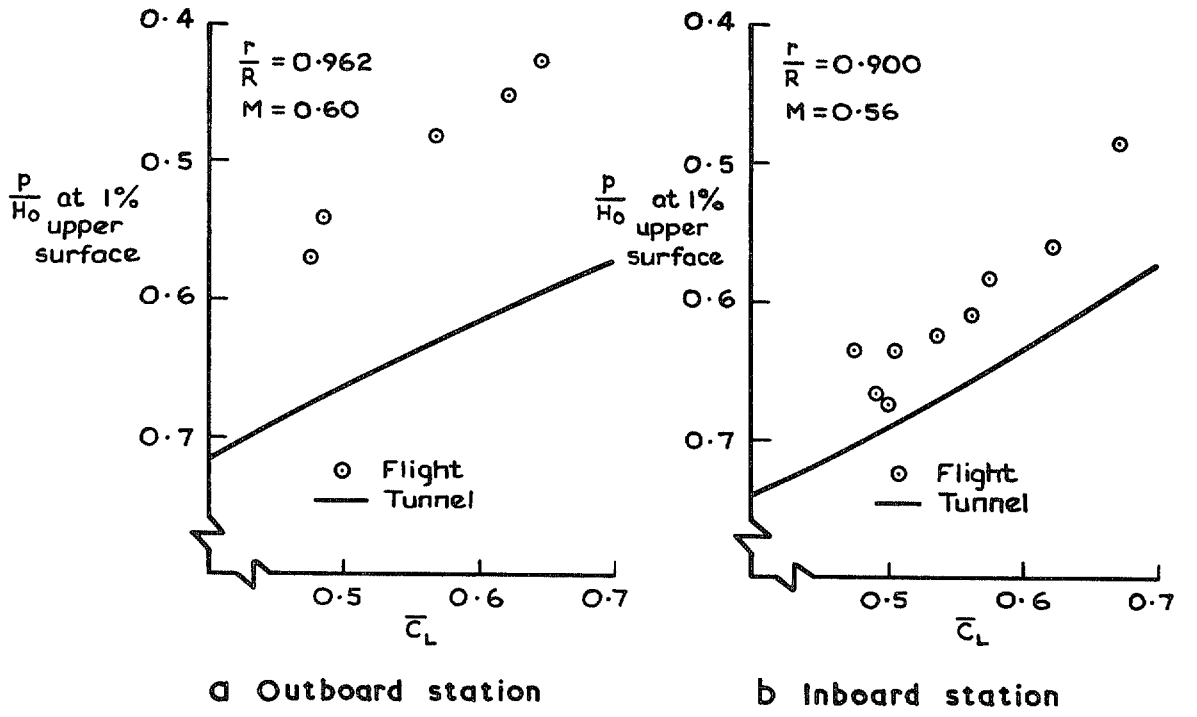

FIG. 21a, b. Comparison of the 0·01 chord pressures with wind tunnel measurements at two spanwise stations for the RAE(NPL) 9615 aerofoil.

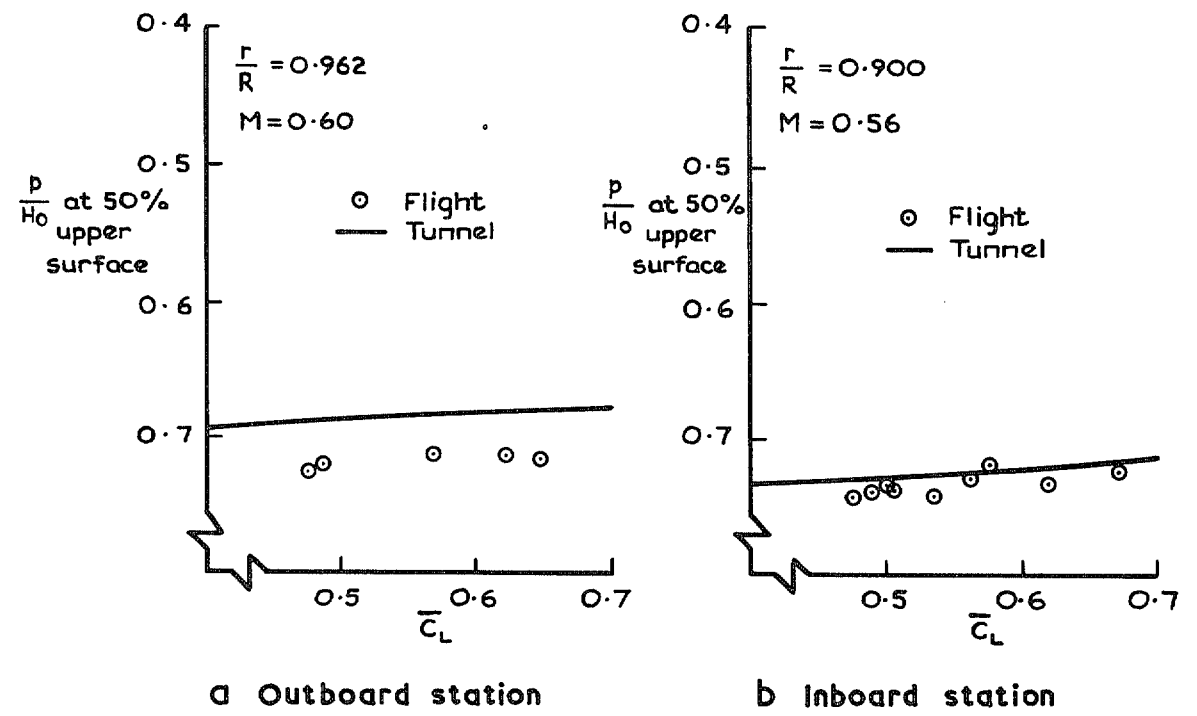

FIG. 22a, b. Comparison of the 0·5 chord pressures with wind tunnel measurements at two spanwise stations for the RAE(NPL) 9615 aerofoil.

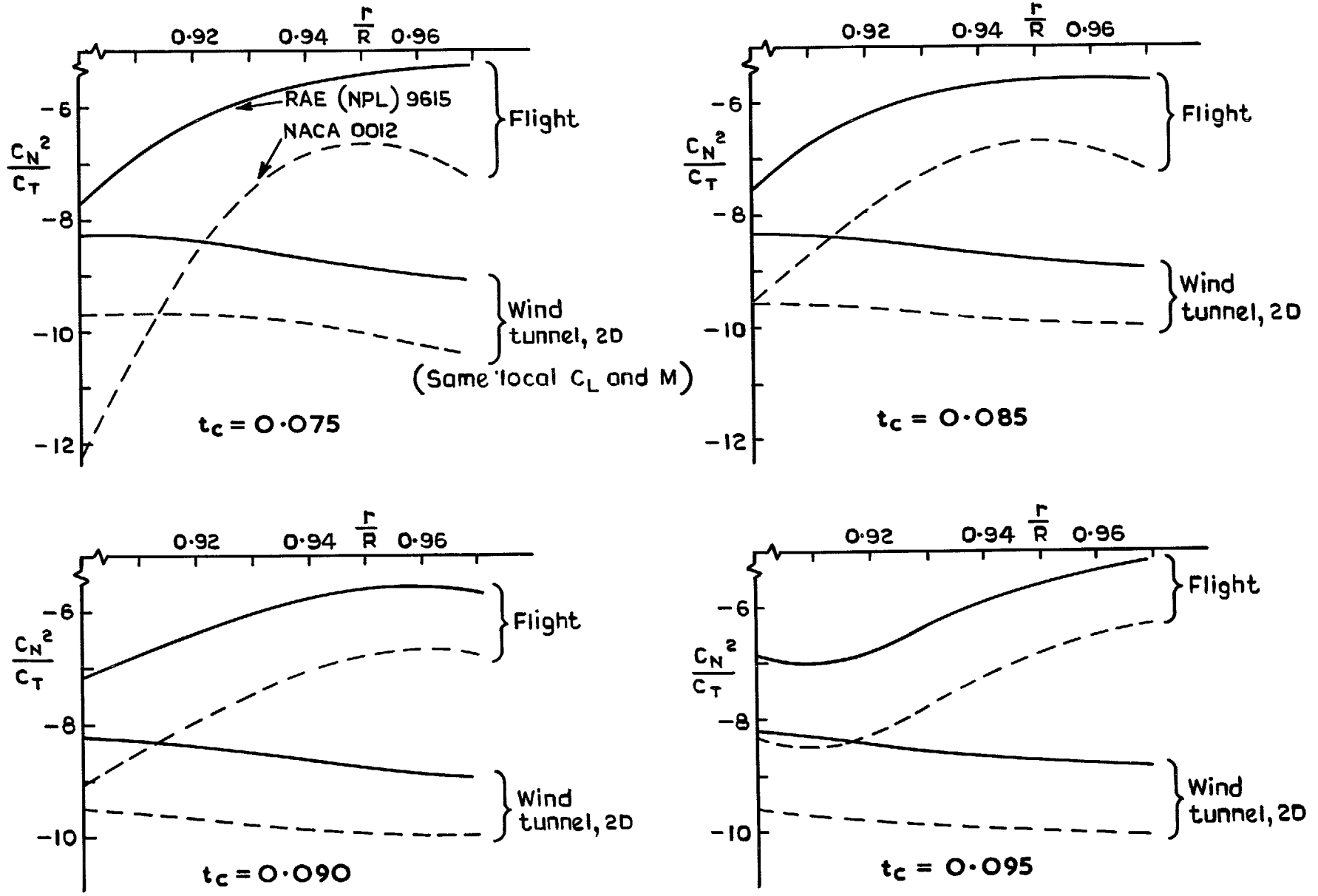

FIG. 23. Values of C_N^2/C_T showing the departure from two-dimensional section characteristics near the blade tip, for four values of the rotor thrust coefficient.

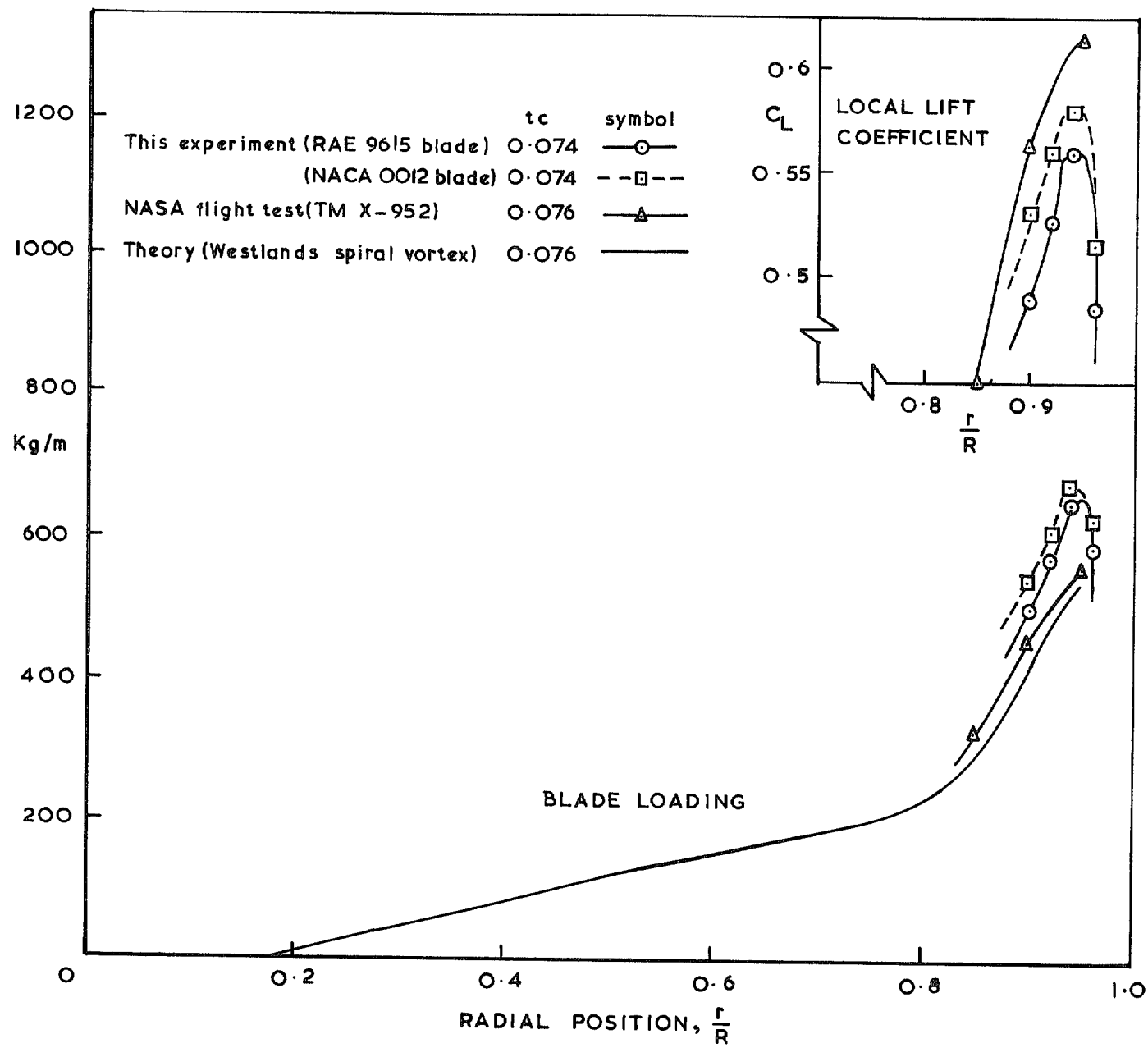

FIG. 24. Mean blade loading measurements showing effect of tip vortex.

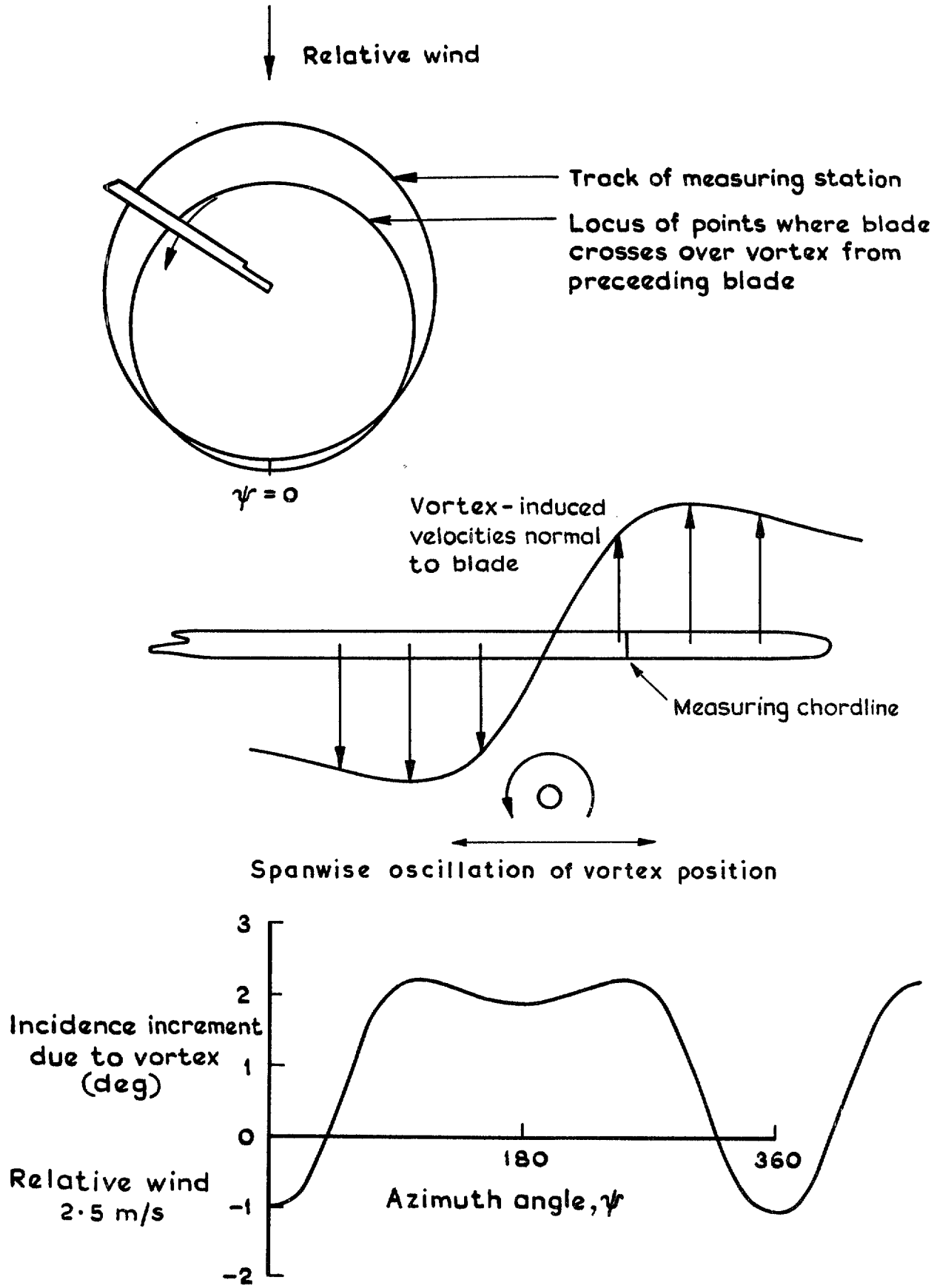

FIG. 25. Line-vortex model of near wake.

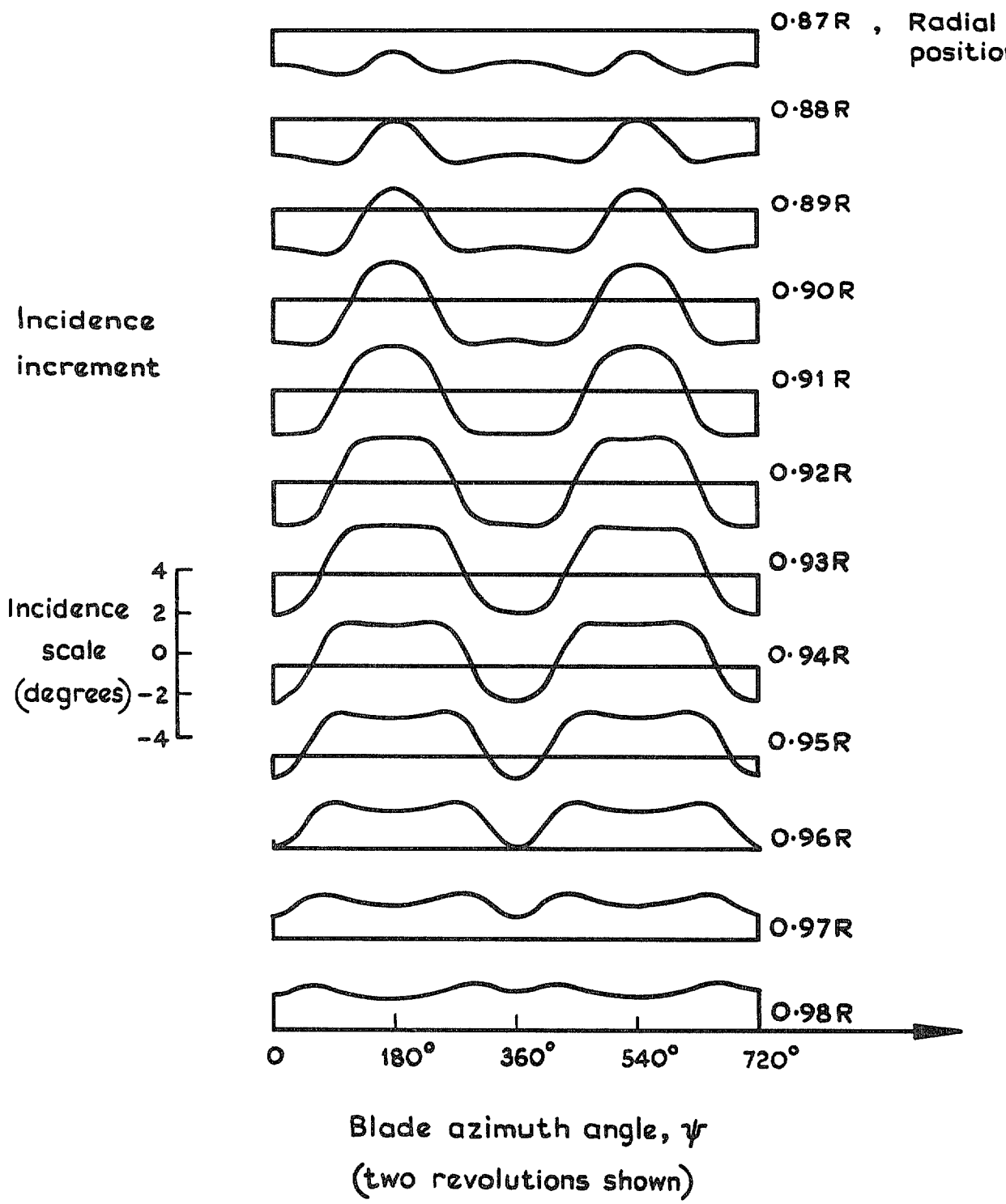

FIG. 26. Incidence increments at a forward speed of 5 knots calculated for a range of radial positions, using the line vortex model.

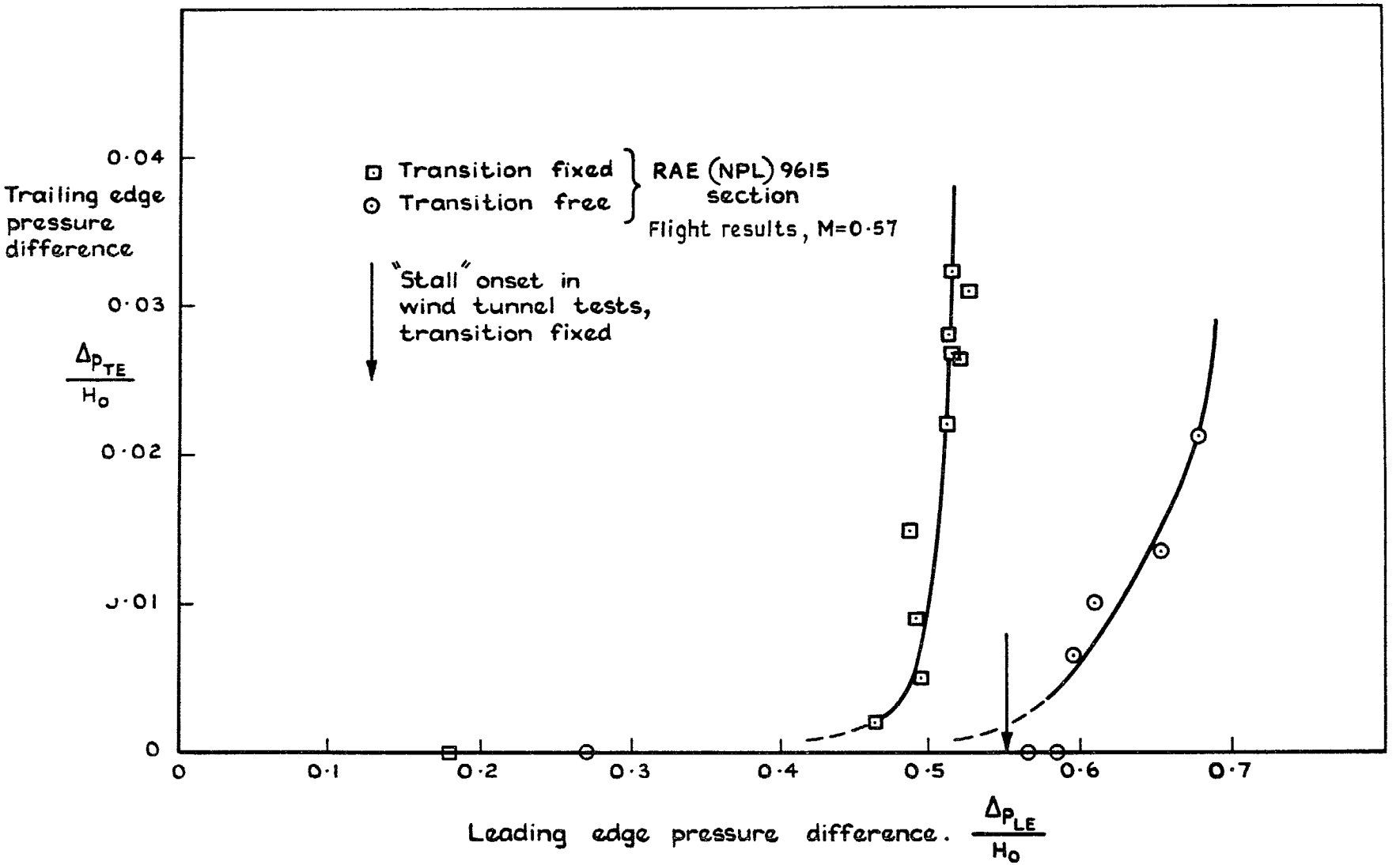

FIG. 27. Stall onset derived from analysis of suction peaks.

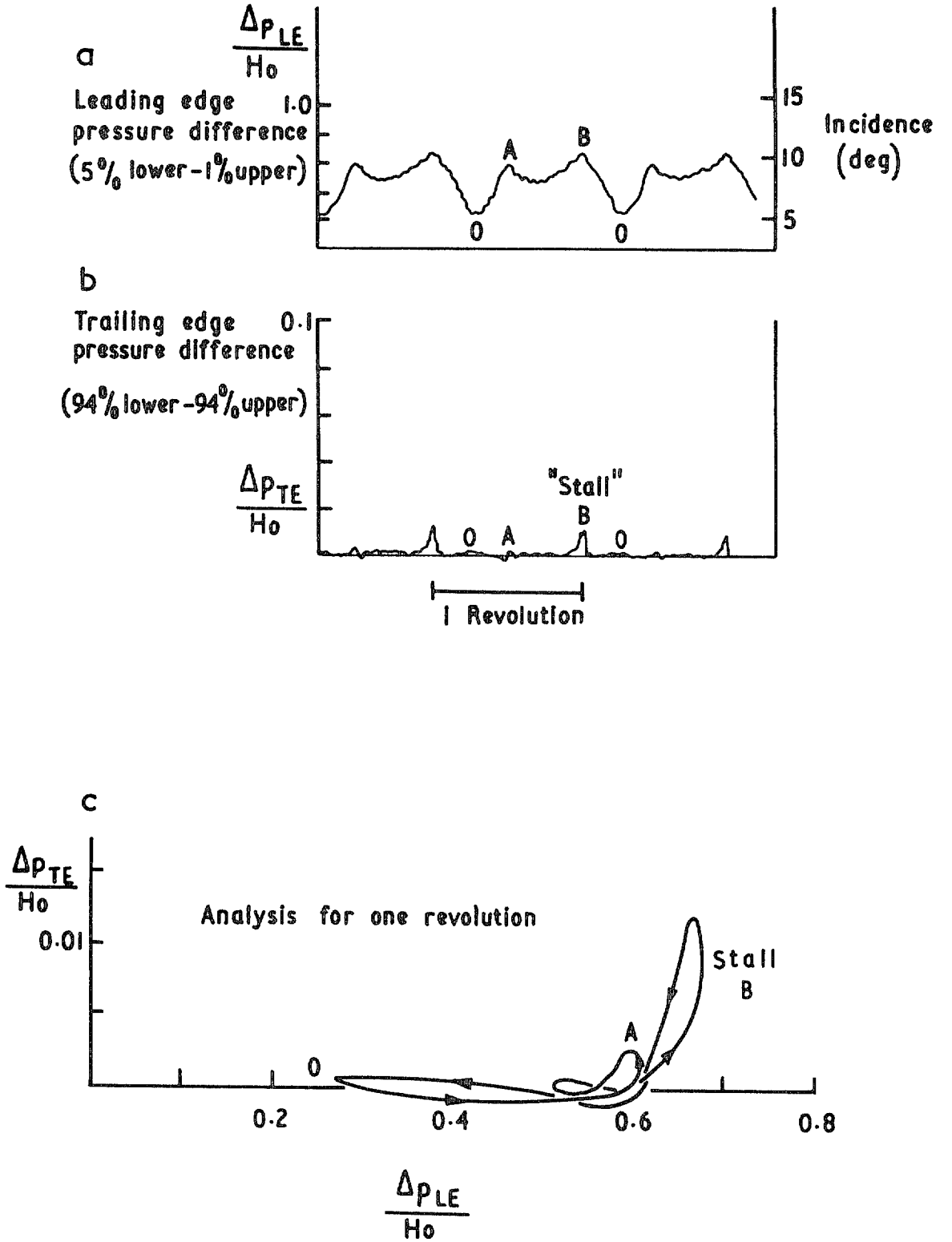

FIG. 28a–c. Cyclic variation of instantaneous pressure differences (transition free).

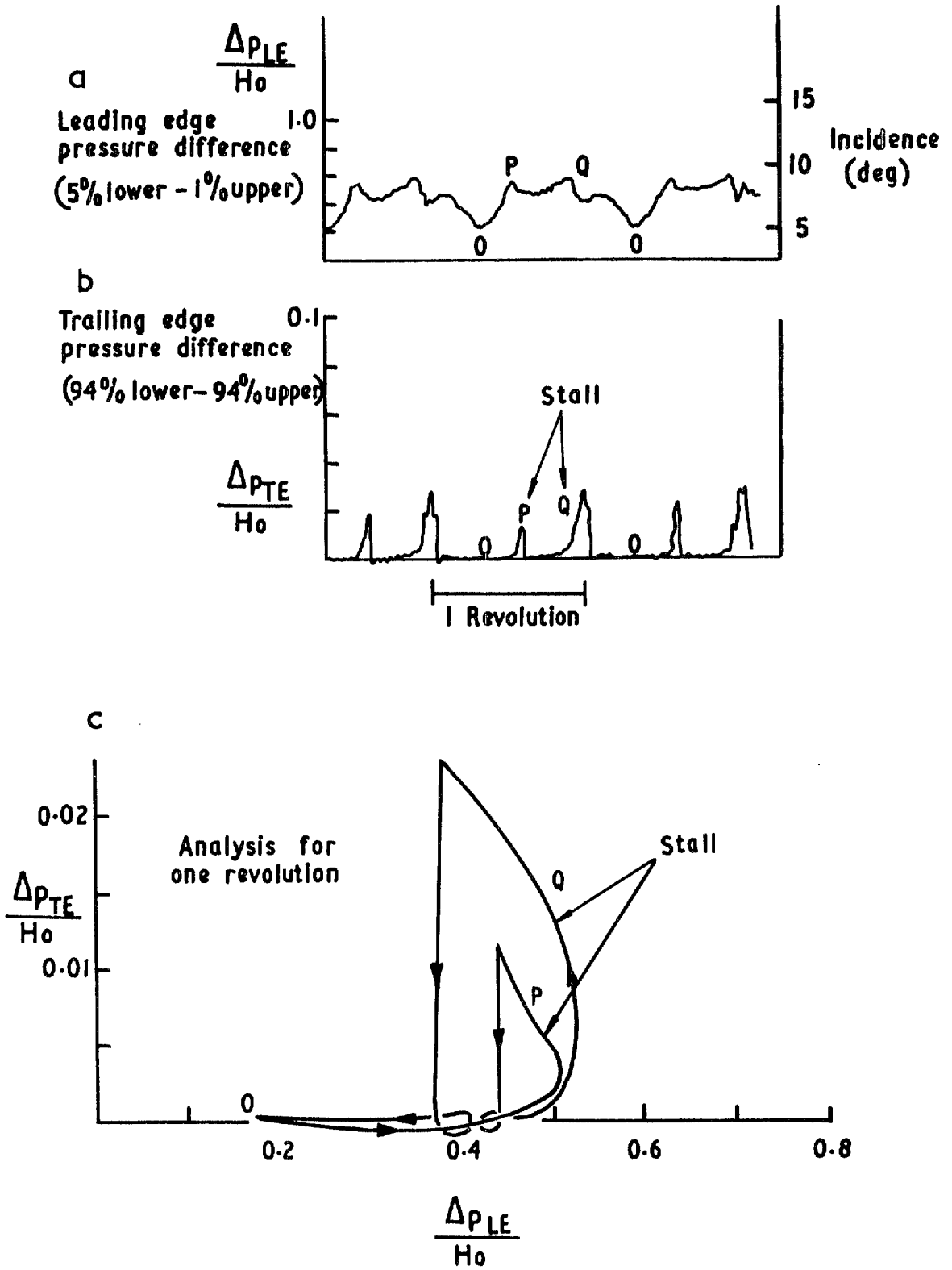

FIG. 29a–c. Cyclic variation of instantaneous pressure differences (transition fixed).

Printed in England for Her Majesty's Stationery Office by J. W. Arrowsmith Ltd., Bristol BS3 2NT
Dd. 290278 K.5. 4/77.

HER MAJESTY'S STATIONERY OFFICE

Bookshops

49 High Holborn, London WC1V 6HB
13a Castle Street, Edinburgh EH2 3AR
41 The Hayes, Cardiff CF1 1JW
Brazennose Street, Manchester M60 8AS
Southey House, Wine Street, Bristol BS1 2BQ
258 Broad Street, Birmingham B1 2HE
80 Chichester Street, Belfast BT1 4JY

Government Publications are also available through Booksellers

R. & M. No. 3792

ISBN 0 11 470963 7